



**QUICKLOOK REPORT:
 QUANTIFICATION OF ROCK
 DAMAGE FROM SMALL
 EXPLOSIONS AND ITS
 EFFECT ON SHEAR-WAVE
 GENERATION**

<p>Weston Geophysical <u>Mark Leidig (Report Preparer)</u> Jessie Bonner James Britton Katherine Murphy Delaine T. Reiter James Lewkowicz Sam Huffstetler</p>		<p>New England Research, Inc. Peter Boyd Randolph J. Martin</p>	
<p>Rock of Ages Corporation Donald Murray Alan Garceau</p>	<p>Maxam North-America Timothy Rath Peter West Jason Trippiedi</p>	<p>Mike's Coring Mike McGinley Amy McGinley</p>	
<p>IRIS PASSCAL Willie Zamora Lisa Foley</p>	<p>Hager-Richter Geoscience Dorothy Richter Rob Garfield Alexis Martinez Jeff Reid</p>	<p>PreSeis Inc. Rob Haas</p>	

August 2008

**Prepared for:
 Air Force Research Laboratory
 AFRL/VSBL
 29 Randolph Road
 Hanscom AFB, MA 01731**

FA8718-08-C-0044

**Prepared By: Weston Geophysical
 181 Bedford Street Suite 1
 Lexington, MA 02420**

REPORT DOCUMENTATION PAGEForm Approved
OMB NO. 0704-0188

Public Reporting burden for this collection of information is estimated to average 1 hour per response, including the time for reviewing instructions, searching existing data sources, gathering and maintaining the data needed, and completing and reviewing the collection of information. Send comment regarding this burden estimates or any other aspect of this collection of information, including suggestions for reducing this burden, to Washington Headquarters Services, Directorate for Information Operations and Reports, 1215 Jefferson Davis Highway, Suite 1204, Arlington, VA 22202-4302, and to the Office of Management and Budget, Paperwork Reduction Project (0704-0188), Washington, DC 20503.

1. AGENCY USE ONLY (Leave Blank)		2. REPORT DATE 31 August 2008	3. REPORT TYPE AND DATES COVERED Interim, July 2008	
4. TITLE AND SUBTITLE Quicklook: Quantification of Rock Damage from Small Explosions and its Effect on Shear-Wave Generation			5. FUNDING NUMBERS FA8718-08-C-0044	
6. AUTHOR(S) Mark Leidig, Jessie Bonner, James Britton, Katherine Murphy, Delaine T. Reiter, James Lewkowicz, Sam Huffstetler, Peter Boyd, Randy Martin, Don Murray, Alan Garceau, Timothy Rath, Peter West, Jason Trippiedi, Mike McGinley, Amy McGinley, Willie Zamora, Lisa Foley, Dorothy Richter, Rob Garfield, Alexis Martinez, Jeff Reid., and Rob Haas.				
7. PERFORMING ORGANIZATION NAME(S) AND ADDRESS(ES) Weston Geophysical Corporation 181 Bedford St., Suite 1 Lexington, MA 02420			8. PERFORMING ORGANIZATION REPORT NUMBER WG-QL0801	
9. SPONSORING / MONITORING AGENCY NAME(S) AND ADDRESS(ES) Air Force Research Laboratory AFRL/VSBL 29 Randolph Road Hanscom AFB, MA 01731			10. SPONSORING / MONITORING AGENCY REPORT NUMBER	
11. SUPPLEMENTARY NOTES The views, opinions and/or findings contained in this report are those of the author(s) and should not be construed as an official U.S. Air Force or U.S. Government policy or decision, unless so designated by other documentation.				
12 a. DISTRIBUTION / AVAILABILITY STATEMENT UNLIMITED			12 b. DISTRIBUTION CODE	
13. ABSTRACT (Maximum 200 words) We conducted the experimental phase of the New England Damage Experiment (NEDE) in a granite quarry near Barre, VT during the first three weeks of July 2008. The goal of this experiment is to characterize the damage from an explosive source and to identify the source(s) of shear wave generation. We hope to quantify crack nucleation and growth (Ashby and Sammis, 1990) as an <i>S</i> -wave generation mechanism in the far field (Sammis, 2002) and to map the cone of damage (Patton et al. 2005; Stevens et al. 2003) above a source, modeled by a compensated linear vector dipole (CLVD). The velocity of explosive detonation (VOD) plays a role in the amount of damage. A faster VOD generates higher pressures that crush the rock into a powder, which inhibits the explosive gasses from driving long cracks. We detonated black powder, ANFO/Emulsion, and COMP B, which have significantly different VOD so we could compare and contrast the damage from each source. Five shots were detonated ranging in size from 134 to 270 lbs of explosives. Over 140 seismic sensors were installed from less than 5 m to 30 km from the blasts specifically to record this experiment. Pre- and post-blast studies of the source rock properties were conducted using acoustic and optical borehole televiewers, coring, and cross-hole tomography.				
14. SUBJECT TERMS Explosions, shear-wave generation, nuclear monitoring, rock damage			15. NUMBER OF PAGES 75	
			16. PRICE CODE	
17. SECURITY CLASSIFICATION OR REPORT UNCLASSIFIED	18. SECURITY CLASSIFICATION ON THIS PAGE UNCLASSIFIED	19. SECURITY CLASSIFICATION OF ABSTRACT UNCLASSIFIED	20. LIMITATION OF ABSTRACT UNLIMITED	

TABLE OF CONTENTS

TABLE OF CONTENTS.....	3
LIST OF FIGURES	4
LIST OF TABLES.....	7
CHAPTER 1. INTRODUCTION	8
Objective.....	8
Location	8
CHAPTER 2. SEISMIC DEPLOYMENTS	13
Near-Source Array.....	13
Short Period 3C Linear Arrays	17
Texan Network.....	21
Video Camera	25
CHAPTER 3. EXPLOSIONS IN BARRE GRANITE.....	27
Shot Characteristics	27
Velocity of Detonation.....	29
Surface Effects.....	33
Peak Particle Velocities	37
CHAPTER 4. SEISMIC DATA EXAMPLES AND ANALYSES.....	39
Near-Source	39
Short Period Linear Arrays.....	41
Texans.....	43
CHAPTER 5. PRE- AND POST-BLAST SOURCE ROCK CHARACTERIZATION.....	48
Core Samples	48
Televiewer.....	49
Cross-hole Tomography.....	54
CHAPTER 6. ACKNOWLEDGMENTS	55
CHAPTER 7. REFERENCES	56
APPENDIX A. HUDDLE TEST.....	57
APPENDIX B. L22 IN-SITU RESPONSE	63
APPENDIX C. L4-3D FACTORY REPSONSE.....	64
APPENDIX D. DATA RECORDS WITH HIGH NOISE OR CONTAMINATION.....	74
Near-source.....	74
Short Period	74
Texan.....	74
APPENDIX E. BLASTER’S LOG FOR 11 JULY 2008 PRODUCTION SHOT	75

LIST OF FIGURES

Figure 1. Rheology surrounding an underground explosion (after Rodean (1971) and modified by Sammis for acoustic fluidization from Melosh, 1979)).	9
Figure 2. Photograph of 3-5 m thick relatively-unfractured sections of Barre granite. The test site was located behind this granite ledge.	10
Figure 3. Geologic map from the Vermont Geological Survey. The black box highlights Barre, VT and the Barre granite igneous intrusion to the southeast. Source: http://www.anr.state.vt.us/DEC/GEO/images/geo5.JPG	11
Figure 4. Location of the test site and alternative test site in relation to nearby structures.	12
Figure 5. Photo of the highly-fractured nature of the granite at the alternative test site (see Figure 4) and a contact with large xenoliths at the abandoned test site.	12
Figure 6. Test site station N1 (blue triangles) and shots (red stars). N1 consisted of two Endeveco accelerometers. N1A remained stationary for all 5 shots, while N1B moved to be less than 5 m from each shot. Station N2 and the camera are also shown on a hill overlooking the test site. (Google Earth Background)	14
Figure 7. Near-source stations N1-N7 (white triangle with red outline) and Texans NT01-NT27 (white dot with red outline). N1 consisted of two sensors, one of which moved for each shot (Figure 6). The shots (white stars with black outline) can be seen in the middle of the image. (Google Earth Background)	15
Figure 8. Example of near-source instrument installation. Katherine Murphy levels and orients a TerraTek accelerometer to true north while Sam Huffstetler installs the Reftek 72A-08 digitizer and battery.	16
Figure 9. A second example of installing a near-source accelerometer and seismometer (Delaine Reiter, Sam Huffstetler, and Mark Leidig).	16
Figure 10. Linear array short period stations (blue triangles) and Texans (red triangles).	18
Figure 11. Discussing where to place the station with the landowner of Carrier's Sky Park.	20
Figure 12. Example of orienting to true north and leveling an L4-3D sensor on the NE line.	20
Figure 13. (Left) RT-125 "Texan" seismic recorder and attached 4.5 Hz vertical spike geophone (orange). For the experiment, the recorder was placed in a plastic bag, laid on its side in a trench, and everything was buried. (Right) Texans in their carrying crates being programmed prior to deployment.	22
Figure 14. Camera overlooking the test site.	26
Figure 15. Loading of ANFO/Emulsion explosive.	28
Figure 16. COMP B charge and the tube taped on to hold the detonator.	28
Figure 17. Lowering the COMP B charge into the hole.	29
Figure 18. Blast plug (white ball) used to help stem the holes.	30
Figure 19. Caliper logs from each blast borehole.	31
Figure 20. Black powder VOD of 0.49 km/s (1608 ft/s) from Shot 1.	32
Figure 21. ANFO/Emulsion VOD of 5.26 km/s (17256 ft/s) from Shot 4.	32
Figure 22. COMP B VOD of 8.31 km/s (27267 ft/s) from Shot 5.	33
Figure 23. Digitized still images of the Shot 1 detonation. Note the two fractures developing after 0.8 s and the further fractures after 1.2 s in the red ellipses.	33
Figure 24. Largest crack generated by Shot 1.	34

Figure 25. Digitized still images of the Shot 2 detonation. Three fractures develop in the white granite flour at 0.8 s and a larger opening releases a plume of gases to the right of the flour at 1.4 s.	34
Figure 26. Digitized still images of the Shot 3 denotation. There were no observable surface effects other than dust on the hilltop camera.	34
Figure 27. Digitized still images of the Shot 4 denotation. This shot produced significantly more dust than Shots 1-3. There may be small amounts of gas release in the gravel pile after 0.8 s, but there were no large fractures observable on the video like for Shots 1 and 2.	35
Figure 28. Crack from Shot 4 observed while walking around the borehole.	35
Figure 29. Digitized still images of the Shot 5 denotation. The PVC pipe begins to leave the borehole at 0.6 s and hits the ground at 6.6 s after detonation. No observable fractures were noted in the video.	36
Figure 30. PVC pipe breaking on guy line during free fall after being ejected from a nearby borehole during Shot 5.	37
Figure 31. Vibration limits set by the U.S. Bureau of Mines (red dashed lines), the predicted values from our blasts (thin blue solid and dashed lines), distance to the nearby structures (thick vertical blue lines), and actual values from previous experiments (multi-colored circles). The peak particle velocities measured at the three structures from the NEDE blasts are shown as yellow stars.	38
Figure 32. Near-source phenomenology for all five shots recorded on sensor N1B about 5 m from each blasthole collar. These data are not plotted on the same amplitude scales in order to better show the characteristics of the initial shock wave, the -1 g spall, and the spall slapdown(s). Figure 33 provides a better representation of the relative amplitudes between the shots.	39
Figure 33. All five shots recorded on the L4-3D vertical channel of station N6. The data were scaled to the maximum amplitude on Shot 5.	40
Figure 34. Vertical, radial, and transverse data of shots 1, 2, and 3 recorded on an L4-3D at station N7.	40
Figure 35. Shot 5 vertical recordings on the short period linear array from north (top) to south (bottom) band passed from 1-4 Hz showing the surface waves.	41
Figure 36. Shot 5 vertical recordings on the short period linear array from north (top) to south (bottom) band passed from 4-10 Hz showing the <i>P</i> and <i>S</i> (?) waves.	42
Figure 37. Shot 5 vertical recordings on the short period linear array from north (top) to south (bottom) high passed above 10 Hz showing the <i>P</i> waves and <i>P</i> - and <i>S</i> - coda.	42
Figure 38. Rayleigh waves at station NE02 for all five shots. Vertical data is band passed between 0.5 and 4 Hz. Note decreasing amplitude of the Rayleigh waves from black powder (Shot 1) to ANFO/Emulsion (shots 2 and 4) to COMP B (shots 3 and 5). The waveforms are color coded by shot size, black=135 lbs, red=270 lbs.	43
Figure 39. NE Texan line band passed from 4 to 10 Hz.	44
Figure 40. SE Texan line band passed from 4 to 10 Hz.	44
Figure 41. Seismic stations in New England that recorded some of the NEDE blasts (star).	45
Figure 42. Love waves recorded on the BHT component of LBNH for Shot 4 (black) and Shot 5 (red). The later part of the wave train may be Rayleigh-waves that have scattered onto the transverse components. However, the first part of the wave train is definitely SH motion.	46
Figure 43. Rayleigh-waves recorded on the BHZ component at LBNH from Shots 4 (black) and 5 (red).	46

Figure 44. Shots 4 (black) and 5 (red) recorded at PKME (280 km). Note the impulsive arrival at group velocity 4 km/s only on the Shot 4 record.	47
Figure 45. Diagram showing the initial planning for geophysical logging of the source rock before and after the explosions.	48
Figure 46. Typical layout of blast hole (SH4), core hole (CH-2), and cross-hole tomography holes (XH4-1 and XH4-2) for all five shots.	49
Figure 47. Example of unfractured core taken from the test site.	50
Figure 48. Compressional wave velocity determined in laboratory study of core taken from near Shot 2. The diametrals indicate orientation in the core hole.	50
Figure 49. Compressional wave velocity as a function of azimuth in the Barre granite near Shot 2. The fast direction is oriented $\sim 30^\circ$ east of true north and is believed to follow the “rift” of the granite.	51
Figure 50. Logging with acoustic and/or optical televiewer.	52
Figure 51. Optical and acoustic televiewer log documenting fractures in the granite.	53
Figure 52. Grout collapsed around PVC pipe in a cross-hole tomography bore hole.	54
Figure 53. Huddle test in the Weston Geophysical parking lot prior to the experiment.	57
Figure 54. "Flip test" for Endeveco sensors.	59
Figure 55. "Flip test" for TerraTek sensors.	59
Figure 56. Near-source vertical L4-3D components.	60
Figure 57. Near-source north/south L4-3D components.	60
Figure 58. Near-source east/west L4-3D components.	61
Figure 59. Weston L4-3D vertical component huddle data for all sensors.	61
Figure 60. PASSCAL L22 vertical component huddle data for all sensors.	62
Figure 61. Comparison of Weston L4-3D (red) and PASSCAL L22 (black) vertical huddle data between 2 and 20 Hz after converting all data to velocity (cm/s).	62
Figure 62. L4-3D L41161 factory calibration specifications.	64
Figure 63. L4-3D L41162 factory calibration specifications.	65
Figure 64. L4-3D L41163 factory calibration specifications.	66
Figure 65. L4-3D L41164 factory calibration specifications.	67
Figure 66. L4-3D L41165 factory calibration specifications.	68
Figure 67. L4-3D L41166 factory calibration specifications.	69
Figure 68. L4-3D L41167 factory calibration specifications.	70
Figure 69. L4-3D L41168 factory calibration specifications.	71
Figure 70. L4-3D L41169 factory calibration specifications.	72
Figure 71. L4-3D L41170 factory calibration specifications.	73

LIST OF TABLES

Table 1. Near-source 3C Sensors.....	13
Table 2. Near-Source Recording Parameters.....	14
Table 3. Station N3 Timing Corrections.....	17
Table 4. Short Period Linear Array Stations.....	19
Table 5. Short Period Recording Parameters.....	19
Table 6. RT-125 “Texan” Sensors.....	22
Table 7. Texan Recording Parameters.....	25
Table 8. Camera Locations.....	25
Table 9. Origin Characteristics for NEDE Shots.....	27
Table 10. Velocity of Detonation.....	32
Table 11. PPVs Measured by PreSeis, Inc.....	38
Table 12. Structures in the Granite of Core Hole 1.....	52
Table 13. Huddle Test Setup.....	58
Table 14. Short Period Data Quality Issues.....	74
Table 15. Texan Data Quality Issues.....	74

CHAPTER 1. INTRODUCTION

Weston Geophysical Corporation, New England Research Inc., and a variety of blasting and geotechnical consultants conducted the experimental field phase of the New England Damage Experiment (NEDE) in a granite quarry near Barre, VT during the first three weeks of July 2008. The goal of this experiment was to characterize the damage around an explosion and to identify possible source(s) of shear wave generation. The velocity of explosive detonation (VOD) and resulting borehole pressures have been shown to play a role in the amount of damage from an explosion*. A faster VOD generates higher pressures that crush the rock into a powder, which inhibits the explosive gasses during the crack forming processes. We detonated various types of explosives with significantly different VOD so we could examine the quantity of damage from each source. Seismic sensors were installed specifically to record this experiment. Pre-blast studies of the source rock properties were conducted and will be compared to currently on-going post-blast studies so that the damage generated by the explosions can be quantified. We have begun initial analyses of the data to quantify the shear wave generation. The goal of this report is to document the field project and the data collected.

Objective

Recent advances in explosion source theory point to the damage that occurs near an explosion as a prominent source of *S*-wave energy. The Ashby and Sammis (1990) model for crack nucleation and growth has been used to predict *S*-wave generation in the far field (Figure 1; Sammis, 2002). Modeling by Patton et al. (2005) and Stevens et al. (2003a) have shown the importance of the cone of damage above a source, modeled by a compensated linear vector dipole (CLVD), in generating *Rg* in the near field and *S* (*Lg*) in the far field, respectively. The phenomenology in the CLVD regime includes block motions, crack damage, and spallation. The NEDE was conducted to test these theories and provide empirical data to aid answering the questions regarding shear wave generation.

Location

The NEDE was conducted in the Barre granite, a homogenous hard rock with low fracture density (Figure 2), to allow study of the damage zones and fractures created by a fully confined and contained explosion. Figure 3 shows a general geologic map of Vermont with a black box showing the location of the Barre granite. The geology of Vermont is an extension of the Appalachian Mountains with structural trends that generally run in a north to northeast orientation. The Barre granite is a felsic intrusion into Silurian to Devonian age rocks of the Connecticut Valley-Gaspé Basin caused by melting due to closing of a basin and collision of continental landmasses (Doolan, 1996). Geologically recently, significant reshaping of the land occurred under thick ice sheets.

* <http://www.johnex.com.au/index.php?section=105> (last accessed in July 2008).

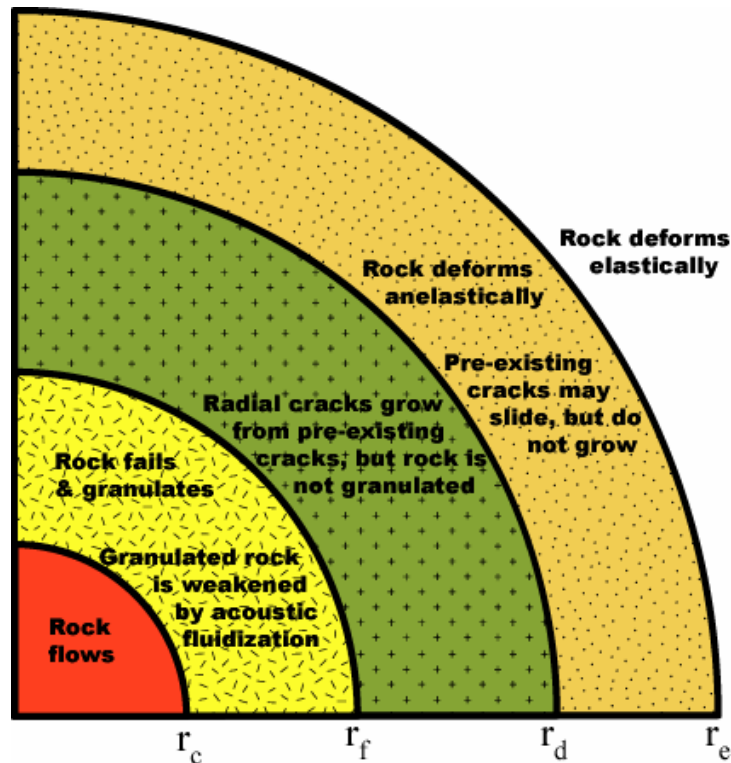


Figure 1. Rheology surrounding an underground explosion (after Rodean (1971) and modified by Sammis for acoustic fluidization from Melosh, 1979).

The fine-grained Barre grey granite has been quarried for over 100 years as a monument stone due its low fracture density and homogeneous composition. While coring the granite for our test applications, the driller often had to snap the core from the bottom of the hole due to a lack of naturally occurring fractures. A further discussion of the Barre granite and its rock properties can be found in CHAPTER 5. PRE- AND POST-BLAST SOURCE ROCK CHARACTERIZATION. A site near the active quarry pit was originally chosen for the blasts (Figure 4). The upper 50 feet of fractured and weathered granite had been stripped off at this site, which allowed us to be closer in depth to the relatively-unfractured, monument-quality Barre granite. Unfortunately, this site was too close to a nearby cell/radio tower and the active quarry wall to detonate our planned 400 lb explosions.

Core drilling at an alternative test site (Figure 4) was conducted further away from the active quarry wall and a nearby cell/radio tower. The alternative site would be far enough away from the sensitive structures so that the planned 400 lb blasts could be safely detonated. Unfortunately, the granite had a much higher fracture density (it was quarried for aggregate stone) and drilling encountered large schistosity xenoliths (Figure 5). This site was abandoned and the experiment was returned into the original location (Figure 4). In order to reduce the projected ground vibrations at the cell/radio tower and high wall of the active quarry to safe limits, we scaled the planned explosions down to ~200 lbs.



Figure 2. Photograph of 3-5 m thick relatively-unfractured sections of Barre granite. The test site was located behind this granite ledge.

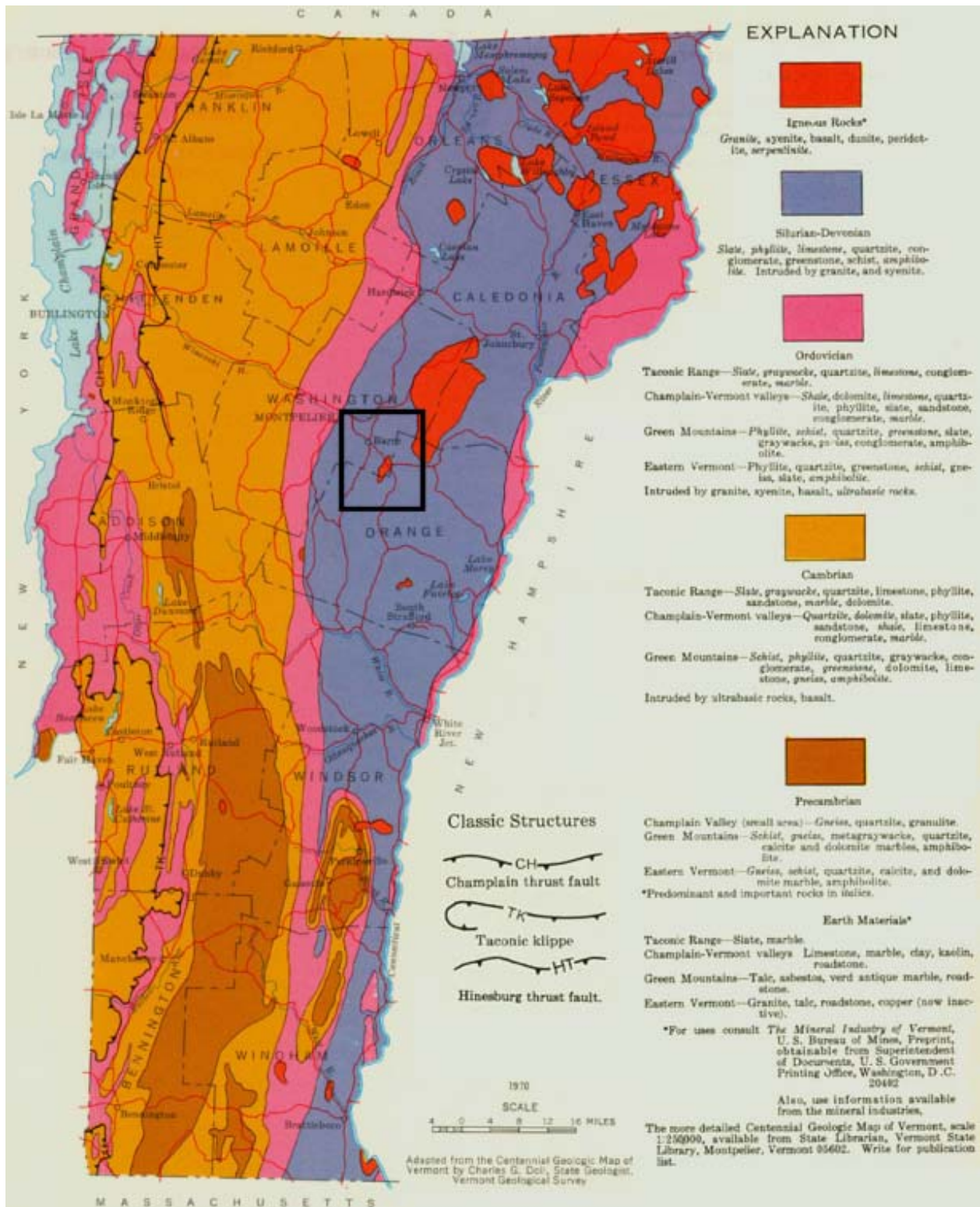


Figure 3. Geologic map (modified) from the Vermont Geological Survey. The black box highlights Barre, VT and the Barre granite igneous intrusion to the southeast. Source: <http://www.anr.state.vt.us/DEC/GEO/images/geo5.JPG>

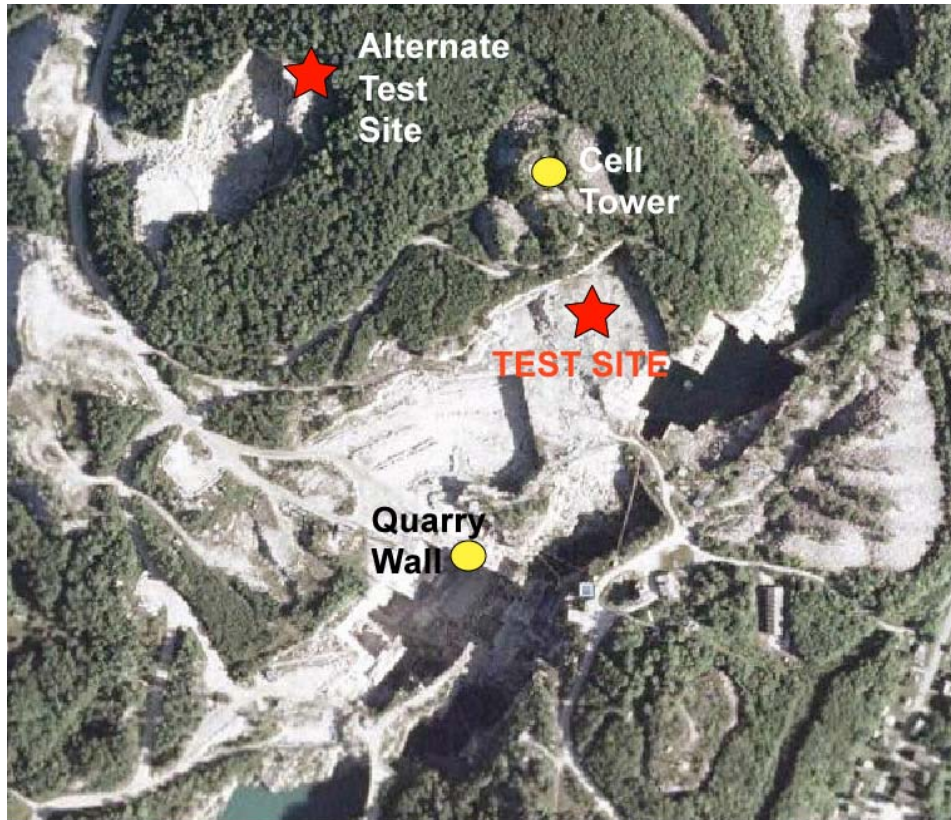


Figure 4. Location of the test site and alternative test site in relation to nearby structures.



Figure 5. Photo of the highly-fractured nature of the granite at the alternative test site (see Figure 4) and a contact with large xenoliths at the abandoned test site.

CHAPTER 2. SEISMIC DEPLOYMENTS

The NEDE explosions were recorded on over 140 seismic instruments, including short-period seismometers, high-g accelerometers, and a high-resolution video camera, deployed at distances of less than 5 m to 30 km from the explosions. We recovered 99.7% of the data.

Near-Source Array

Jessie Bonner, James Britton, Katherine Murphy, Sam Huffstetler, Delaine Reiter, and Mark Leidig (Weston) deployed 6 short period Mark Product L4-3D seismometers, 2 Endevco 100 g accelerometers, and 5 TerraTek 40 g accelerometers in close proximity to the explosions to record the source phenomenology. All of these instruments recorded three components (3C) of motion. One of the accelerometers (N1B) was moved before each shot to be less than 5 m from the borehole to record shot time. In addition to acquiring shot time, these near-source data will be used in moment tensor inversions. Table 1 lists the locations and instrumentation deployed for the three-component near-source array. Figure 6 shows the locations of the very close-in sensors and the shot locations. The remainder of the near-source stations, at distances of less than 1 km, can be seen in Figure 7.

Station N5 was across an 80 m deep quarry pit (Don Murray, pers. comm.), now filled with water. This pit may have an effect on the data at station N5 and the data for some shots at station N4. Station N2 was deployed above the test site on the edge of a high wall.

Table 1. Near-source 3C Sensors.

Station	Latitude	Longitude	Elev (m)	Channels 1-3	S/N	Channels 4-6	S/N	DAS	DISK	GPS
N1A	44.15785	-72.47808	503	Endevco	6			734	5715	663
N1B Shot 1	44.15782	-72.47852	501			Endevco	2	734	5715	663
N1B Shot 2	44.15803	-72.47814	508			Endevco	2	734	5715	663
N1B Shot 3	44.15783	-72.47773	507			Endevco	2	734	5715	663
N1B Shot 4	44.15749	-72.47793	506			Endevco	2	734	5715	663
N1B Shot 5	44.15752	-72.47753	503			Endevco	2	734	5715	663
N2	44.15826	-72.47862	533	L4-3D	189	TerraTek	7	738	87	664
N3	44.15724	-72.47930	492	L4-3D	257	TerraTek	9	716	5106	248
N4	44.15642	-72.47736	500	L4-3D	619	TerraTek	8	733	5959	669
N5	44.15687	-72.47575	506	L4-3D	37	TerraTek	6	739	5247	674
N6	44.15967	-72.48204	489	L4-3D	L41168			940F		4196
N7	44.15637	-72.47913	502	L4-3D	628	TerraTek	4	743	5713	244

The near-source accelerometers and seismometers were placed in a shallow hole, oriented to true north, and lightly covered with dirt. True north was 16° west of magnetic north at our location for the experiment. For placement of the Endevco accelerometers, very shallow holes were dug into the granite with a rock bar. The sensors were coupled to the granite with dirt and granite flour from the drilling. Data were recorded at 250 sps on 24-bit Reftek 72A-08 DAS for all stations except N6, which was digitized on a Reftek RT130. More recording parameters can be found in Table 2. The DAS (and hard drive if applicable) and GPS clock were placed in a plastic

tub and covered by a garbage bag. The external GPS clock acquired GMT time. A 17 Ah deep-cycle battery powered each station. Figure 8 and Figure 9 show examples of the sensors being installed and the plastic tub with recording equipment. Information on the near-source vertical-component only sensors shown in Figure 7 can be found in the following “Texan Network” section.

Table 2. Near-Source Recording Parameters.

Parameter	Value
Digitizer	Reftek 72A-08 (N1-N5, N7) Reftek RT130 (N6)
Channels	Reftek 72A-08 – 6 Reftek RT130 – 3
Resolution	24-bit
Gain	1
Sample Rate	250
Record Mode	Continuous
Data Format	Reftek 72A-08 – PASSCAL [†] 32 bit Reftek RT130 – PASSCAL Compressed



Figure 6. Test site station N1 (blue triangles) and shots (red stars). N1 consisted of two Endeveco accelerometers. N1A remained stationary for all 5 shots, while N1B moved to be less than 5 m from each shot. Station N2 and the camera are also shown on a hill overlooking the test site. (Google Earth Background)

[†] Program for Array Seismic Studies of the Continental Lithosphere



Figure 7. Near-source stations N1-N7 (white triangle with red outline) and Texans[‡] NT01-NT27 (white dot with red outline). N1 consisted of two sensors, one of which moved for each shot (Figure 6). The shots (white stars with black outline) can be seen in the middle of the image. (Google Earth Background)

[‡] “Texans” refer to single-component geophones recorded on a small digitizer with internal memory and power. The name “Texan” refers to the original design by Stever Harder, who worked for a university in Texas.



Figure 8. Example of near-source instrument installation. Katherine Murphy levels and orients a TerraTek accelerometer to true north while Sam Huffstetler installs the Reftek 72A-08 digitizer and battery.



Figure 9. A second example of installing a near-source accelerometer and seismometer (Delaine Reiter, Sam Huffstetler, and Mark Leidig).

Station N3 had a timing issue. It is unclear whether this was a problem with the DAS or clock, but at the beginning of a new data file, the time would jump 1 second forward and then back. This would happen a few times for each file. Arrivals at N3 came in late by an increasing number of seconds with respect to the other near-source stations. The offsets seem to be in terms of full seconds as the millisecond accuracy appears to be correct, but I cannot verify this. Corrections to the processed data have been applied by the amounts shown in Table 3. Station N3 should not be used in the development of the velocity model.

Table 3. Station N3 Timing Corrections.

Shot	Correction (sec)
1	3
2	5
3	7
4	11
5	14

Short Period 3C Linear Arrays

Two linear arrays of short-period 3C seismometers were deployed extending away from the test site for 30 km in two directions as shown in Figure 10 and Table 4. Station spacing was designed to be every 3 km “as the crow flies” from the test site. A lack of roads and many inaccessible areas, particularly along the NE line, made maintaining station spacing and a straight line difficult. Station NE06 was not deployed due to a 6 km region void of any roads. The NE line followed the trend of the granite intrusives and the structural trend of the region (Figure 3), while the SE line cut across the structural trend. The stations were generally located along dirt roads that only saw local resident traffic. Vehicle traffic can be seen in the recordings, and passing cars interfered with a few recordings. Permissions were obtained to install these sensors from the local Vermont towns, but several stations along the NE line required landowner permission as well (Figure 11).

Nine Sercel (formerly Mark Products) 1 Hz L4-3D short period seismometers with Reftek RT130 digitizers were installed along the NE line by Mark Leidig, James Britton, and Katherine Murphy (Weston) and Lisa Foley (PASSCAL). Along the SE line, ten Mark Products 2 Hz L22 short period seismometers were installed by Jessie Bonner, Sam Huffstetler, Delaine Reiter (Weston) and Willie Zamora (PASSCAL). All stations had an external GPS clock for recording GMT time and recorded at 250 sps. More recording information can be found in Table 5.

The sensors were oriented to truth north, placed in a shallow hole, leveled, and loosely covered with soil (Figure 12). The soil was generally an organic rich dense soil, but sometimes had large amounts of decaying plant matter that left the site somewhat “spongy”. No solid bedrock was found at the sites within a foot of the surface. Therefore, it is expected that site responses will have some variation. A huddle test was conducted prior to the experiment and that information can be found in Appendix A. PASSCAL collected in-situ response information for each of the L22s on the SE line. This information can be found in Appendix B. Lisa Foley examined the in-situ data and found sensor 496L (SE02) had a “bad” channel 2 and thinks that a faulty internal

connection is the cause. Initial examination of the data did not show any abnormalities with this sensor. She also noted the examination of the 462L (SE08) sensor found swapped and reversed cables, which made the north/south channel into the east/west channel and vice versa. The polarity on each channel was also flipped. Response information for the Sercel L4-3Ds can be found in Appendix C.

The RT130 digitizer, GPS clock, and 79 AH deep-cycle battery were placed in a black plastic bag and hidden behind bushes or covered with grass and leaves for camouflage. The GPS clock was held upright by attaching the sensor cable to the DAS through the metal clock loop. At a couple sites, tall grass interfered with satellite reception and the clock was elevated by placing it on top of foam pads that were placed on the battery box.

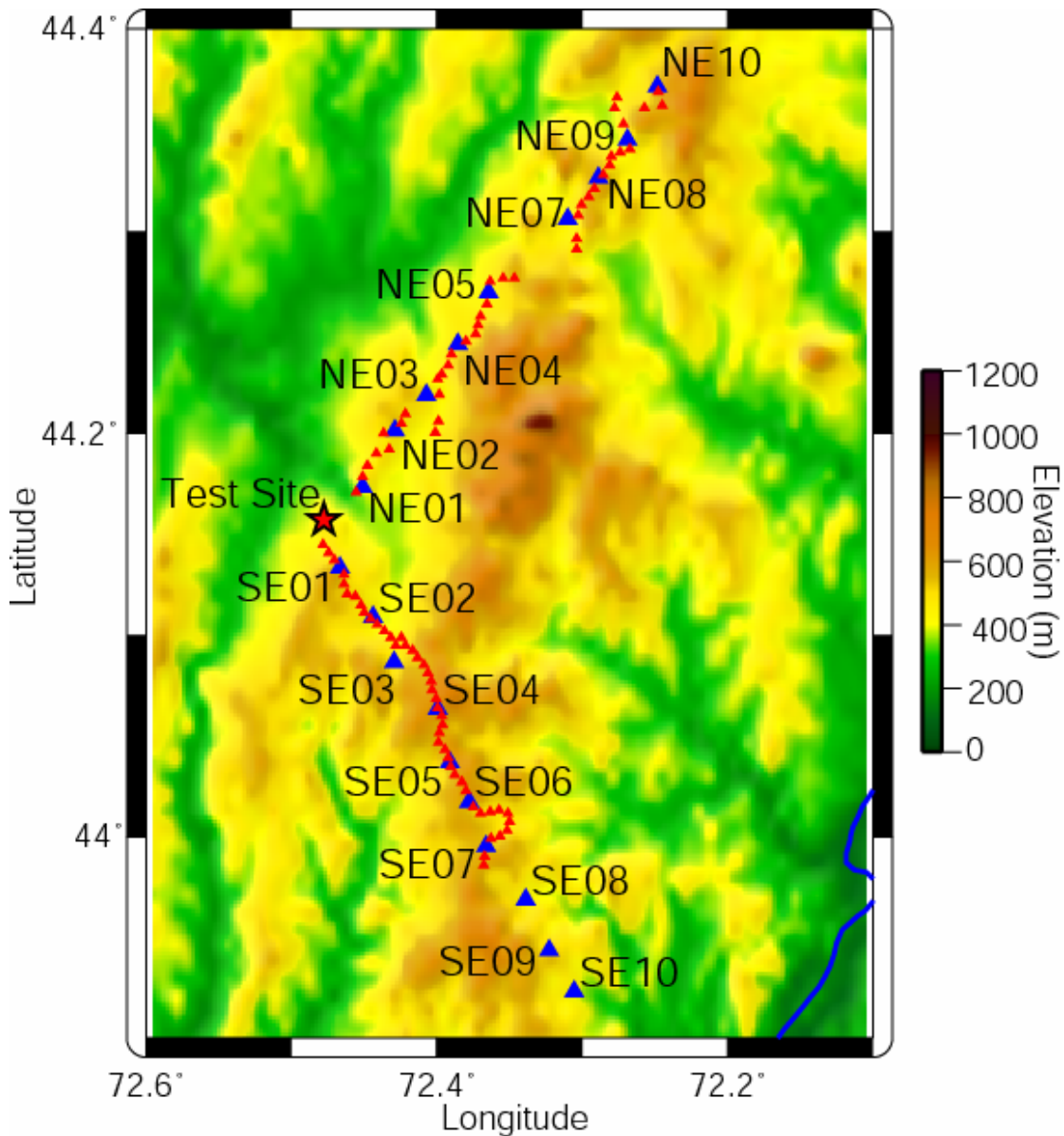


Figure 10. Linear array short period stations (blue triangles) and Texans (red triangles).

Table 4. Short Period Linear Array Stations.

Station	Latitude	Longitude	Elev (m)	Channels 1-3	S/N	DAS	GPS
SE01	44.13362	-72.46659	514	L22	459L	9D63	5155
SE02	44.10946	-72.44367	475	L22	496L	A198	4161
SE03	44.08698	-72.42968	470	L22	479L	9669	4188
SE04	44.06350	-72.39923	595	L22	494L	9E50	4176
SE05	44.03733	-72.39093	588	L22	720L	939E	4175
SE06	44.01771	-72.37772	514	L22	643L	930E	3890
SE07	43.99543	-72.36589	556	L22	449L	9E45	4194
SE08	43.96925	-72.33883	456	L22	462L	9D42	4198
SE09	43.94373	-72.32292	507	L22	642L	9312	4179
SE10	43.92329	-72.30565	369	L22	468L	9E40	4189
NE01	44.17376	-72.45101	420	L4-3D	L41167	9E4B	2449
NE02	44.20178	-72.42899	511	L4-3D	L41166	9D8F	2565
NE03	44.21921	-72.40699	474	L4-3D	L41169	9DEA	2514
NE04	44.24436	-72.38558	462	L4-3D	L41162	9E18	2711
NE05	44.26989	-72.36425	447	L4-3D	L41164	9E1B	2531
NE07	44.30621	-72.30992	436	L4-3D	L41161	9E42	2661
NE08	44.32654	-72.28904	541	L4-3D	L41165	9E4F	2665
NE09	44.34530	-72.26903	461	L4-3D	L41170	9DAA	2516
NE10	44.37157	-72.24832	542	L4-3D	L41163	9E17	2520

Table 5. Short Period Recording Parameters.

Parameter	Value
Digitizer	Reftek RT130
Channels	3
Resolution	24-bit
Gain	32
Sample Rate	250
Record Mode	Continuous
Data Format	PASSCAL Compressed
Sensor	1 Hz Sercel L4-3D (NE01-NE10) 2 Hz Mark L22 (SE01-SE10)
Sensitivity	Appendices B and C



Figure 11. Discussing where to place the station with the landowner of Carrier's Sky Park.



Figure 12. Example of orienting to true north and leveling an L4-3D sensor on the NE line.

Texan Network

Weston Geophysical and IRIS PASSCAL split into three teams and deployed 112 Reftek RT-125 “Texans” (Figure 13) along the NE and SE short period array lines and around the test site (Figure 7 and Figure 10). Two of the 112 Texans deployed either had a cable or geophone problem. Data was successfully retrieved from every other instrument in the experiment. The Texan stations are single channel sensors with a 4.5 Hz 3” spike vertical geophone and were installed every 0.5 km along the short period array lines. Willie Zamora and Lisa Foley scouted a possible third line to the west of the test site, but found the road and traffic conditions unfavorable.

The team along the SE line (Sam Huffstetler, Delaine Reiter, and Willie Zamora) installed sensors every 0.5 km of driving mileage, including in close proximity to the short period sensors. Therefore, they installed 45 Texans in about 22 km of distance. Their stations are named ST01-ST45.

The NE line Texan team (Mark Leidig, Katherine Murphy, and James Britton) installed the Texans every 0.5 km as the crow flies with respect to the test site and skipped sites that fell near the already installed short period sensors. They were only able to install 40 Texans (NT01-NT40) along their 30 km line with this method because they were confronted with inaccessible regions where no Texans could be placed.

Jessie Bonner, Lisa Foley, and Sam Huffstetler formed the third team and installed 27 Texans around and in the test region (NT01-NT27). These Texans will be helpful in examining any possible radiation patterns generated by the shots.

Table 6 lists the Texan locations and Table 7 details the recording parameters. The Texans were programmed the morning of installation by Willie Zamora to record during specified time intervals for 4 days at 250 sps (Table 7). The recorder was placed in a small plastic bag, to keep it clean, and then placed in a shallow trench. The geophone was placed vertically in the ground using a bubble level and everything was covered with dirt to hide them and provide thermal stability. The recorders were powered by two internal Duracell Procell D size batteries that were installed prior to programming. Since all shots were completed in one day, the sensors were pulled on day two of recording, acquisition was stopped, and the data were dumped.



Figure 13. (Left) RT-125 “Texan” seismic recorder and attached 4.5 Hz vertical spike geophone (orange). For the experiment, the recorder was placed in a plastic bag, laid on its side in a trench, and everything was buried. (Right) Texans in their carrying crates being programmed prior to deployment.

Table 6. RT-125 “Texan” Sensors.

Station	Latitude	Longitude	Elev (m)	Geophone	S/N
NT01	44.14975	-72.47660	439	4.5 Hz	1847
NT02	44.15050	-72.47139	474	4.5 Hz	1817
NT03	44.15306	-72.46688	469	4.5 Hz	2185
NT04	44.15661	-72.46726	433	4.5 Hz	2988
NT05	44.15994	-72.46902	419	4.5 Hz	2137
NT06	44.16267	-72.47063	399	4.5 Hz	2148
NT07	44.16375	-72.47424	402	4.5 Hz	2087
NT08	44.16403	-72.47813	411	4.5 Hz	3003
NT09	44.16295	-72.48178	446	4.5 Hz	2455
NT10	44.16111	-72.48428	450	4.5 Hz	2218
NT11	44.15758	-72.48488	483	4.5 Hz	2237
NT12	44.15627	-72.48574	471	4.5 Hz	2703
NT13	44.15452	-72.48631	445	4.5 Hz	2464
NT14	44.15202	-72.48542	415	4.5 Hz	1910
NT15	44.15061	-72.48338	424	4.5 Hz	2450
NT16	44.14973	-72.47993	436	4.5 Hz	2161
NT17	44.14983	-72.47882	430	4.5 Hz	2465
NT18	44.15044	-72.47791	441	4.5 Hz	2459
NT19	44.15135	-72.47785	469	4.5 Hz	1919
NT20	44.15220	-72.47769	478	4.5 Hz	2142
NT21	44.15300	-72.47834	481	4.5 Hz	2589
NT22	44.15392	-72.47892	485	4.5 Hz	1555
NT23	44.15469	-72.47827	488	4.5 Hz	2564

Station	Latitude	Longitude	Elev (m)	Geophone	S/N
NT24	44.15552	-72.47762	491	4.5 Hz	2179
NT25	44.15637	-72.47777	489	4.5 Hz	1923
NT26	44.15683	-72.47819	488	4.5 Hz	1683
NT27	44.15724	-72.47828	508	4.5 Hz	1522
ST01	44.14481	-72.47836	415	4.5 Hz	2155
ST02	44.14083	-72.47468	470	4.5 Hz	2089
ST03	44.13749	-72.47077	501	4.5 Hz	1649
ST04	44.12999	-72.46384	527	4.5 Hz	1739
ST05	44.12524	-72.46401	508	4.5 Hz	2253
ST06	44.12048	-72.46160	525	4.5 Hz	1697
ST07	44.11936	-72.45598	517	4.5 Hz	1836
ST08	44.11476	-72.45226	487	4.5 Hz	1941
ST09	44.11152	-72.45009	476	4.5 Hz	1884
ST10	44.10815	-72.44569	453	4.5 Hz	1718
ST11	44.10532	-72.44118	431	4.5 Hz	1694
ST12	44.10210	-72.43603	432	4.5 Hz	2044
ST13	44.09886	-72.43151	456	4.5 Hz	1868
ST14	44.09502	-72.42836	451	4.5 Hz	2362
ST15	44.09881	-72.42456	480	4.5 Hz	1676
ST16	44.09485	-72.42188	502	4.5 Hz	2990
ST17	44.09256	-72.41641	516	4.5 Hz	2234
ST18	44.08877	-72.41341	528	4.5 Hz	1746
ST19	44.08528	-72.40897	555	4.5 Hz	2476
ST20	44.08119	-72.40638	569	4.5 Hz	1706
ST21	44.07713	-72.40380	598	4.5 Hz	2994
ST22	44.07272	-72.40329	641	4.5 Hz	2153
ST23	44.06861	-72.40077	616	4.5 Hz	1815
ST24	44.06423	-72.39933	605	4.5 Hz	2091
ST25	44.06016	-72.39693	587	4.5 Hz	2477
ST26	44.05563	-72.39617	595	4.5 Hz	2480
ST27	44.05147	-72.39829	599	4.5 Hz	2479
ST28	44.04698	-72.39883	623	4.5 Hz	1790
ST29	44.04327	-72.39462	611	4.5 Hz	1808
ST30	44.03915	-72.39230	600	4.5 Hz	2475
ST31	44.03485	-72.39060	606	4.5 Hz	2566
ST32	44.03075	-72.38752	595	4.5 Hz	2474
ST33	44.02710	-72.38279	604	4.5 Hz	2612
ST34	44.02293	-72.38020	618	4.5 Hz	2837
ST35	44.01464	-72.37524	576	4.5 Hz	2461
ST36	44.01176	-72.37000	535	4.5 Hz	2463
ST37	44.01231	-72.36317	520	4.5 Hz	1655
ST38	44.01310	-72.35706	513	4.5 Hz	2451
ST39	44.01176	-72.35107	474	4.5 Hz	1841
ST40	44.00738	-72.34996	483	4.5 Hz	1784
ST41	44.00307	-72.35169	490	4.5 Hz	2458
ST42	44.00023	-72.35682	505	4.5 Hz	2452

Station	Latitude	Longitude	Elev (m)	Geophone	S/N
ST43	43.99909	-72.36286	518	4.5 Hz	2453
ST44	43.99044	-72.36703	549	4.5 Hz	2457
ST45	43.98604	-72.36784	560	4.5 Hz	2230
TN01	44.17101	-72.45563	357	4.5 Hz	1827
TN02	44.17853	-72.45098	461	4.5 Hz	1702
TN03	44.18431	-72.44757	460	4.5 Hz	1762
TN04	44.19030	-72.44159	464	4.5 Hz	1835
TN05	44.19208	-72.43277	490	4.5 Hz	1899
TN06	44.20009	-72.43657	490	4.5 Hz	1934
TN07	44.20498	-72.42451	486	4.5 Hz	2017
TN08	44.20959	-72.42144	475	4.5 Hz	1634
TN09	44.20053	-72.40111	429	4.5 Hz	1652
TN10	44.20614	-72.39907	419	4.5 Hz	1682
TN11	44.21946	-72.39829	417	4.5 Hz	1750
TN12	44.22675	-72.39961	428	4.5 Hz	1569
TN13	44.22939	-72.39684	463	4.5 Hz	2113
TN14	44.23362	-72.39248	452	4.5 Hz	1567
TN15	44.23918	-72.39013	473	4.5 Hz	1570
TN16	44.24562	-72.38012	470	4.5 Hz	1578
TN17	44.24944	-72.37331	476	4.5 Hz	1612
TN18	44.25382	-72.37190	476	4.5 Hz	1520
TN19	44.25821	-72.36987	455	4.5 Hz	1789
TN20	44.26419	-72.36535	437	4.5 Hz	2478
TN21	44.27529	-72.36361	436	4.5 Hz	1972
TN22	44.27692	-72.35464	493	4.5 Hz	2573
TN23	44.27680	-72.34652	524	4.5 Hz	1677
TN24	44.29133	-72.30389	454	4.5 Hz	1736
TN25	44.29651	-72.30374	445	4.5 Hz	2991
TN26	44.30800	-72.30269	454	4.5 Hz	2562
TN27	44.31292	-72.30035	492	4.5 Hz	2561
TN28	44.31717	-72.29567	523	4.5 Hz	2560
TN29	44.32093	-72.29184	537	4.5 Hz	2572
TN30	44.32799	-72.28578	537	4.5 Hz	2563
TN31	44.33274	-72.28131	504	4.5 Hz	2924
TN32	44.33710	-72.27986	469	4.5 Hz	2927
TN33	44.33886	-72.27404	453	4.5 Hz	2926
TN34	44.34054	-72.26735	441	4.5 Hz	2920
TN35	44.35288	-72.27189	431	4.5 Hz	2902
TN36	44.36076	-72.27804	394	4.5 Hz	2901
TN37	44.36620	-72.27633	437	4.5 Hz	2904
TN38	44.36110	-72.25740	518	4.5 Hz	2874
TN39	44.36218	-72.24525	594	4.5 Hz	2921
TN40	44.36885	-72.24784	565	4.5 Hz	2923

Table 7. Texan Recording Parameters.

Parameter	Value
Digitizer	Reftex RT125
Channels	1 - vertical
Resolution	24-bit
Gain	32
LSB (nV/count)	57.37
Sample Rate	250
Record Mode	Time Windows
Window 1 (UTC)	2008:194:14:00 to 2008:194:24:00
Window 2 (UTC) [§]	2008:195:14:00 to 2008:195:24:00
Window 3 (UTC)	2008:196:19:00 to 2008:196:24:00
Window 4 (UTC)	2008:197:19:00 to 2008:197:24:00
Sensor	4.5 Hz vertical 3" spike

Video Camera

A Sony Hi-8 video camera recorded all of the explosions in order to study the surface manifestations of the explosions. A picture of the camera overlooking the test site is shown in Figure 14. The camera needed to be moved a few feet for Shot 3 to avoid the vantage angle being blocked by vegetation. The camera was moved back to its initial location for shots 4 and 5. The locations of the camera are listed in Table 8 and plotted in Figure 6. The Hi-8 analog videos were digitized to small computer movies. Jessie Bonner also recorded many of the explosions using his personal hand held video camera placed on a tripod near the blasts. Those videos provide a view of the blasts from a different angle.

Table 8. Camera Locations.

Station	Latitude	Longitude	Elev (m)	Shots Recorded
Camera1	44.15837	-72.47800	541	1, 2, 4, 5
Camera2	44.15842	-72.47816	538	3

[§] NOTE: Texan recording stopped on day 195 and data dumped.



Figure 14. Camera overlooking the test site.

CHAPTER 3. EXPLOSIONS IN BARRE GRANITE

Shot Characteristics

We detonated five explosions at the test site on 12 July 2008 (Table 9). A delay-fired production shot was conducted on 11 July 2008, and we have the blasters information for this shot (Appendix E). A goal of this experiment was to examine how the velocity of detonation affects the damage and shear wave generation. Three explosives with dramatically different VOD were used to compare these effects. Our planned single-fired blasts ranged in yield from 134 to 270 lbs of explosives with the first three being ~135 lbs of black powder, ANFO/Emulsion (Heavy ANFO), and Composition B (COMP B), respectively. The blast plan was designed and executed by Mr. Tim Rath of Maxam-North America who was assisted by Peter West and Jason Trippiedi.

Table 9. Origin Characteristics for NEDE Shots.

Shot	Date	Origin Time (GMT)	Latitude	Longitude	Elevation (m)	Borehole/Centroid Depth (m)	Stemming (m)	Yield (lbs)	Explosive
1	7/12/2008 (194)	14:37:42.160	44.15774	-72.47848	509	9.1/8.5	7.3	134	Black Powder
2	7/12/2008 (194)	16:02:05.020	44.15800	-72.47813	509	11.3/10.7	10.1	135.5	ANFO/Emul 50:50
3	7/12/2008 (194)	17:30:40.730	44.15780	-72.47770	503	11.3/10.7	10.4	136	COMP B
4	7/12/2008 (194)	19:16:15.010	44.15751	-72.47797	508	13.7/12.8	11.6	269.5	ANFO/Emul 50:50
5	7/12/2008 (194)	20:50:12.770	44.15754	-72.47757	503	13.7/12.8	11.9	270	COMP B
P1	7/11/2008 (193)	~19:33:54	-	-	-	-	-	-	ANFO

Note: Yield is based on explosives + detonators.

Lat/Long/Elevation error was 4+ meters according to the GPS unit.

Black powder is traditionally used for firearms and fireworks because its slow burn rate produces gases that can propel a bullet but not damage the barrel. It has a low brisance, the rate at which an explosive reaches maximum pressure, which means it generates relatively fewer fractures in the rock around the explosive source. The fractures generated will be longer due to the escape of the explosive gasses. Occasionally, it is used to break monument stone, such as granite, without damaging the stone itself due to properties of gas expansion only along pre-existing cracks.

ANFO/Emulsion (Figure 15) is the primary blasting agent used in the mining industry due to its stability, low cost, easy production as well as optimum blast effects for rock fracturing. ANFO is considered a high explosive when properly confined and especially when mixed with an emulsion. We use the phrase Heavy ANFO to describe the 50:50 ANFO:Emulsion mix used for the NEDE.

Composition B (Figure 16) is a military grade explosive composed of RDX and TNT. It is primarily used in military applications such as munitions. COMP B is a shapeable charge and

was cast specifically to fit our boreholes. One cast charge was used for Shot 3 and two were used for Shot 5. The high VOD of this explosive allowed it to be used in the first nuclear weapons. During the experiment, increased care was required handling this explosive due to its increased sensitivity and the booster being strapped to the charge as it was being lowered down the hole (Figure 17). A small amount of ANFO/Emulsion was poured in the hole prior to loading the COMP B charge to increase explosive coupling to the borehole.



Figure 15. Loading of ANFO/Emulsion explosive.



Figure 16. COMP B charge and the tube taped on to hold the detonator.



Figure 17. Lowering the COMP B charge into the hole.

Table 9 lists the total depth of the boreholes, the centroid depths of the explosive column, and the amount of stemming. Stemming consisted of granite flour from drilling, a blast plug (Figure 18) designed to lock into the borehole walls, and ½” gravel. The boreholes had a 9” diameter as logged by Hager-Richter Geoscience (Figure 19).

The shot time was determined by placing an Endevco accelerometer (N1B) within 5 m of the borehole and examining the first large positive break on the vertical component. With the explosives at a maximum depth of 13 m, the compressional wave took less than three milliseconds to reach the sensor. Time is accurate to better than 0.05 seconds.

Velocity of Detonation

The velocity of detonation (VOD; Table 10) was measured using a MREL HandiTrap II. A resistance wire is taped to the booster and lowered down the hole. As the explosives burn up the borehole, the resistance wire is melted and the recorder measures the decreasing resistance at 1

million samples per second. The resistance was then converted to distance and a velocity calculated.

Black powder burns the slowest with a VOD of 0.49 km/s (1608 ft/s; Figure 20). The ANFO/Emulsion (Figure 21) and COMP B (Figure 22) explosives are considered high explosives due to their 5.26 and 8.31 km/s VOD, respectively. The first ANFO/Emulsion shot detonated with a VOD of 5.06 km/s. It is not clear why there is a VOD difference between these two shots. Explosive confinement can play an important role in explosive performance and may have been a factor. The blaster forgot to attach the VOD resistance wire to Shot 3, the first COMP B charge, as he was focused on safely handling the charge.



Figure 18. Blast plug (white ball) used to help stem the holes.

Table 10. Velocity of Detonation.

Shot	Explosive	VOD (km/sec)
1	Black Powder	0.49
2	ANFO/Emul 50:50	5.06
3	COMP B	-
4	ANFO/Emul 50:50	5.26
5	COMP B	8.31

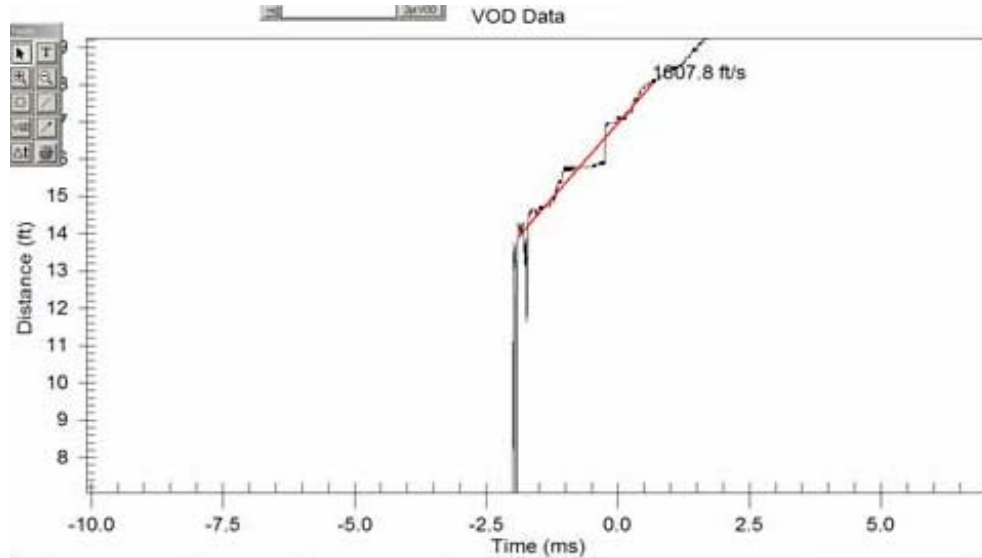


Figure 20. Black powder VOD of 0.49 km/s (1608 ft/s) from Shot 1.

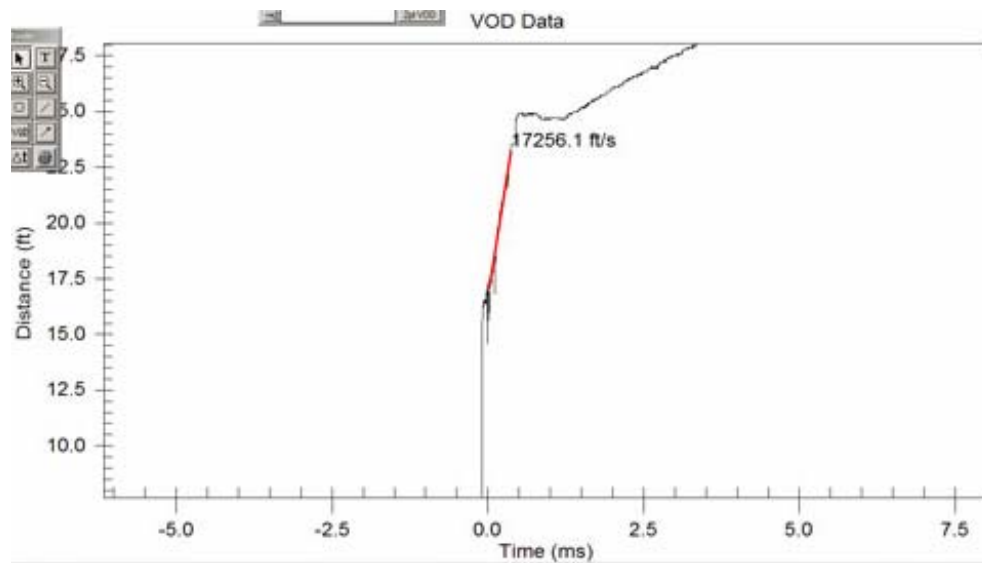


Figure 21. ANFO/Emulsion VOD of 5.26 km/s (17256 ft/s) from Shot 4.

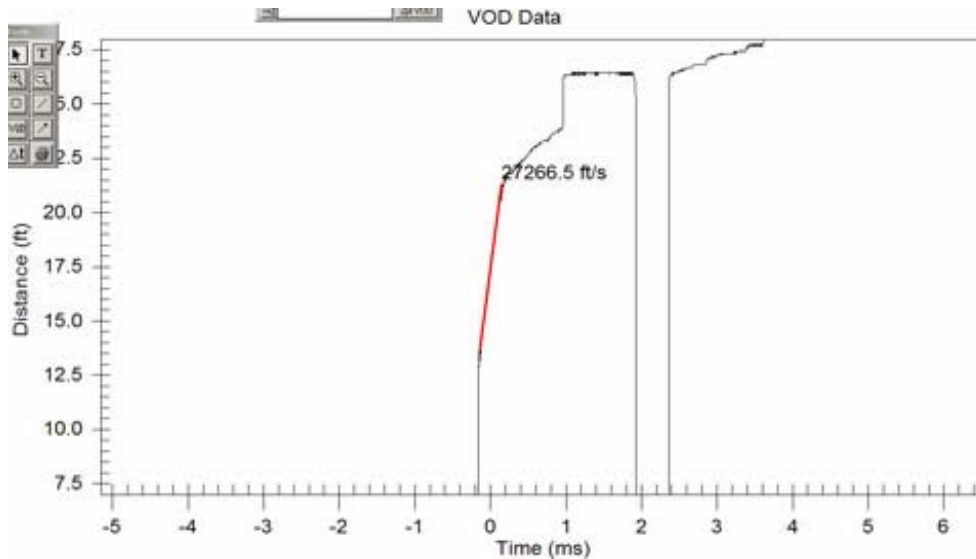


Figure 22. COMP B VOD of 8.31 km/s (27267 ft/s) from Shot 5.

Surface Effects

A Sony Hi-8 video camera (Figure 14) recorded each explosion. The analog video was digitized into mpeg movies available via e-mail from Weston Geophysical Corporation. The video data show the surface processes that occurred during the explosion so that secondary effects of the source can be modeled. All shots spalled, but no shots cratered or produced fly rock. Shot 1 generated the most observable surface fracturing and still video images are shown in Figure 23. A photo of the largest crack generated by Shot 1 is shown in Figure 24. This crack both opened and had vertical displacement of a few centimeters.

Along with the black powder shot, the small ANFO/Emulsion Shot 2 produced some surface fracturing (Figure 25), although the extent was not the same as from Shot 1. Neither Shot 3 (Figure 26) or Shot 4 (Figure 27) produced any surface fracturing visible in the video, although small cracks were observed on the ground after the Shot 4 (Figure 28). The two larger shots, shots 4 and 5, produced significantly more dust.



Figure 23. Digitized still images of the Shot 1 detonation. Note the two fractures developing after 0.8 s and the further fractures after 1.2 s in the red ellipses.



Figure 24. Largest crack generated by Shot 1.



Figure 25. Digitized still images of the Shot 2 detonation. Three fractures develop in the white granite floor at 0.8 s and a larger opening releases a plume of gases to the right of the floor at 1.4 s.



Figure 26. Digitized still images of the Shot 3 denotation. From the hilltop camera, there were no observable surface effects other than dust.



Figure 27. Digitized still images of the Shot 4 detonation. This shot produced significantly more dust than Shots 1-3. There may be small amounts of gas release in the gravel pile after 0.8 s, but there were no large fractures observable on the video like for Shots 1 and 2.



Figure 28. Crack from Shot 4 observed while walking around the borehole.

Two sections of PVC pipe (~20') were ejected from a nearby borehole, used for cross-hole tomography, by the explosive gasses during Shot 5. This hole as well as its partner hole on the other side of Shot 5 ejected large volumes of the bentonite grout. Individual snapshots of the video from Shot 5 are provided in Figure 29. The pipe can be seen leaving the borehole and the grout being ejected beginning 0.6 s and 0.8 s, respectively, after the detonation. Calculations to determine the maximum height attained by the PVC pipe returned values ranging from 20.3 to 45.6 m. The pipe hit a guy line, attached to a quarry tower crane, on the way down (Figure 30) making exact determination of height difficult. Although, we believe it to be approximately 33 m. Gas can be seen shooting from the borehole under high pressure for 4-5 s after the detonation. This loss of containment will affect the amount of gas available for driving fractures in the granite and will have to be taken into account during analyses.

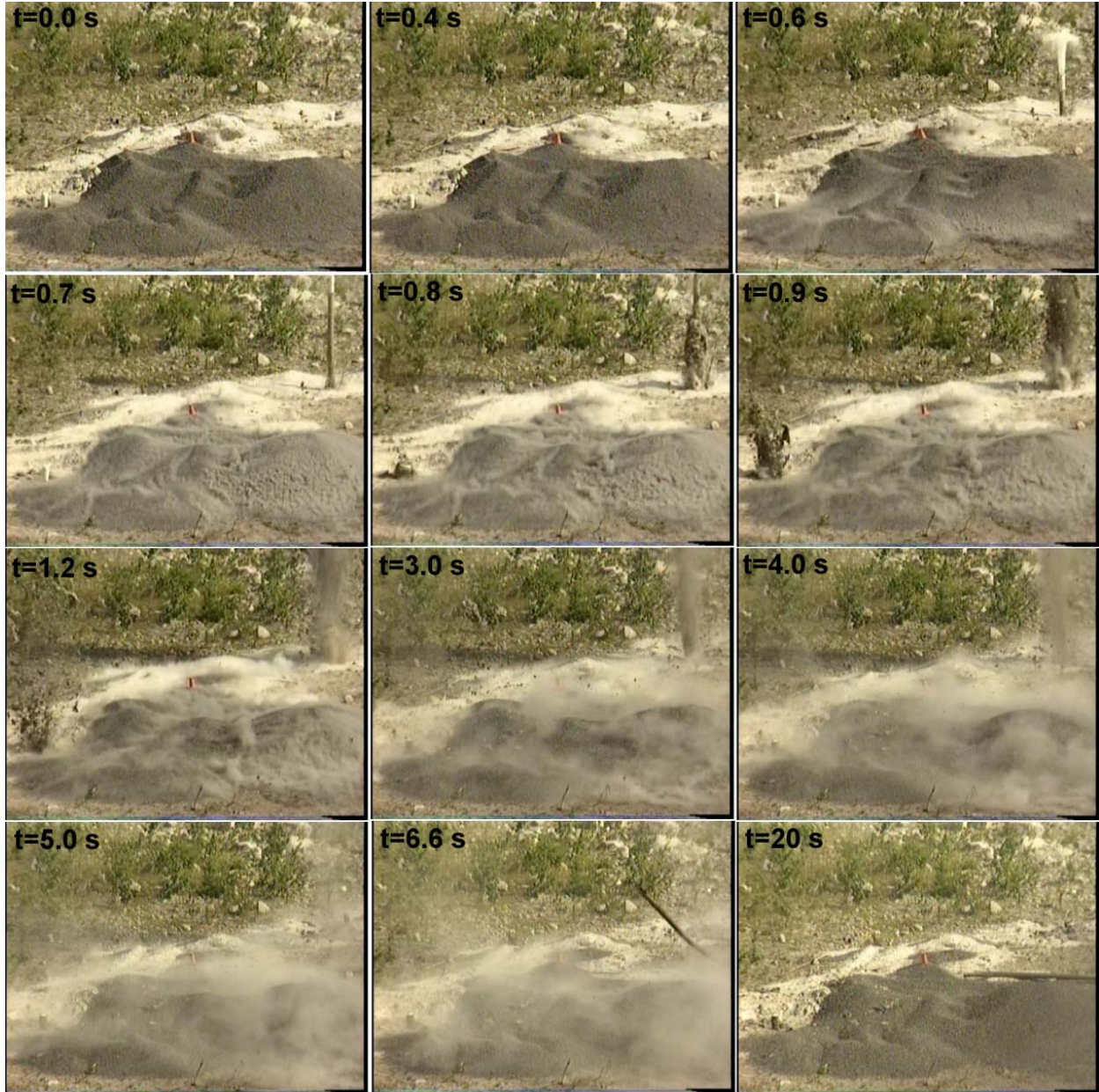


Figure 29. Digitized still images of the Shot 5 denotation. The PVC pipe begins to leave the borehole at 0.6 s and hits the ground at 6.6 s after detonation. No observable fractures were noted in the video.



Figure 30. PVC pipe breaking on guy line during free fall after being ejected from a nearby borehole during Shot 5.

Peak Particle Velocities

The proximity to nearby structures such as a cell/radio tower, the quarry high wall, and quarry cranes constrained the maximum size of the blasts we could conduct. The U.S. Bureau of Mines (USBM) sets peak particle velocity limits (U.S. Bureau of Mines RI 8507, 1980) that we followed. To allow for larger blasts, a second prospective test site was investigated in another region of the mine (Figure 4). Unfortunately, this site contained large xenoliths and the granite did not have a low fracture density (Figure 5).

The site in closer proximity to the tower and quarry structures was chosen due to the quality of granite. The predicted peak particle velocities were calculated to determine the maximum shot size using the following equation:

$$PPV=K*SD^A,$$

where PPV is the peak particle velocity (in/s), K is a site constant (we used 605, the most conservative K value for an overly-confined explosion), SD is scaled distance (ft/lb^{0.5}), and A is another site constant (we used -1.6, a value based on low attenuation media).

The results of applying the planned shot sizes (either 200 or 400 lbs) and test site geometry in the above equation are shown in Figure 31. Also shown are the USBM limits for above and below 10 Hz and observed peak particle velocities from previous Weston Geophysical experiments. The values used in the above equation are very conservative and no prior observed data has been above the predicted values.

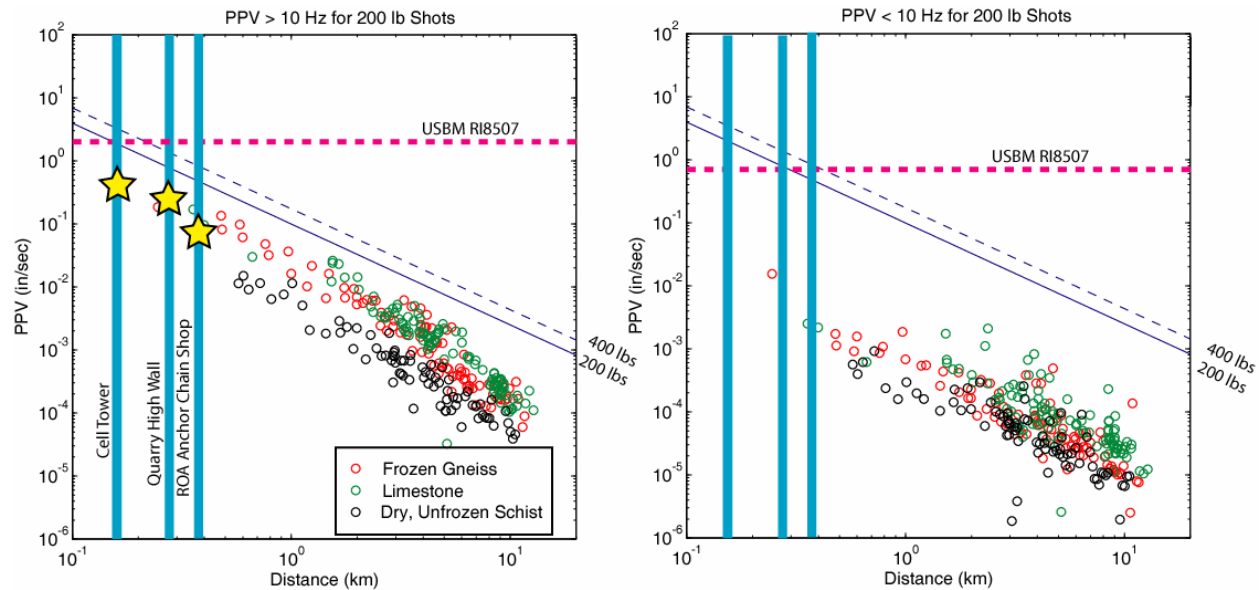


Figure 31. Vibration limits set by the U.S. Bureau of Mines (red dashed lines), the predicted values from our blasts (thin blue solid and dashed lines), distance to the nearby structures (thick vertical blue lines), and actual values from previous experiments (multi-colored circles). The peak particle velocities measured at the three structures from the NEDE blasts are shown as yellow stars.

Rob Haas of PreSeis, Inc. deployed “InstanTel” seismic sensors at the cell/radio tower, quarry high wall, and the World War II anchor chain shop to provide rapid measurements of PPV. The location of the WWII anchor chain shop was close to the nearest residential structure. Our plan was to shoot the smaller shots, measure the PPVs at each site, then decide whether or not to shoot the larger charges as planned or decrease their sizes. Figure 31 compares the observed maximum PPVs from the InstanTels and the predictions. Table 31 shows which NEDE shot provided the maximum seismic vibration and acoustic signal at each structure. The values were all below the estimated PPVs and the USBM limits for safe vibration limits. The data seem to fall along the trend of our measured values from previous explosion experiments.

Table 11. PPVs Measured by PreSeis, Inc

Location	Distance (ft)	Max PPV (in/sec)	Shot #	Max Acoustic (db)	Shot #
Cell/Phone Tower	403	0.420	2	114	4
Quarry Wall	875	0.290	5	114	4
Anchor Chain Shop	1192	0.060	3	105	2

CHAPTER 4. SEISMIC DATA EXAMPLES AND ANALYSES

In this section, we present examples of the waveforms collected during the experiment.

Near-Source

Below are a few examples of the near-source data recordings. In Figure 32 the vertical spall from all five shots is recorded on station N1B. Note the classic spall from Shot 5 with an impulsive shock wave arrival, 0.2 seconds of spall, and then a small spike from the slap down. Shot 4 has a double spike from the shock wave and a longer spall before three smaller slap downs. Shot 1 has a long duration shock wave arrival possibly caused by a “burning” of the explosives column instead of an instantaneous detonation. The origin times for the shots were determined from these data as well.

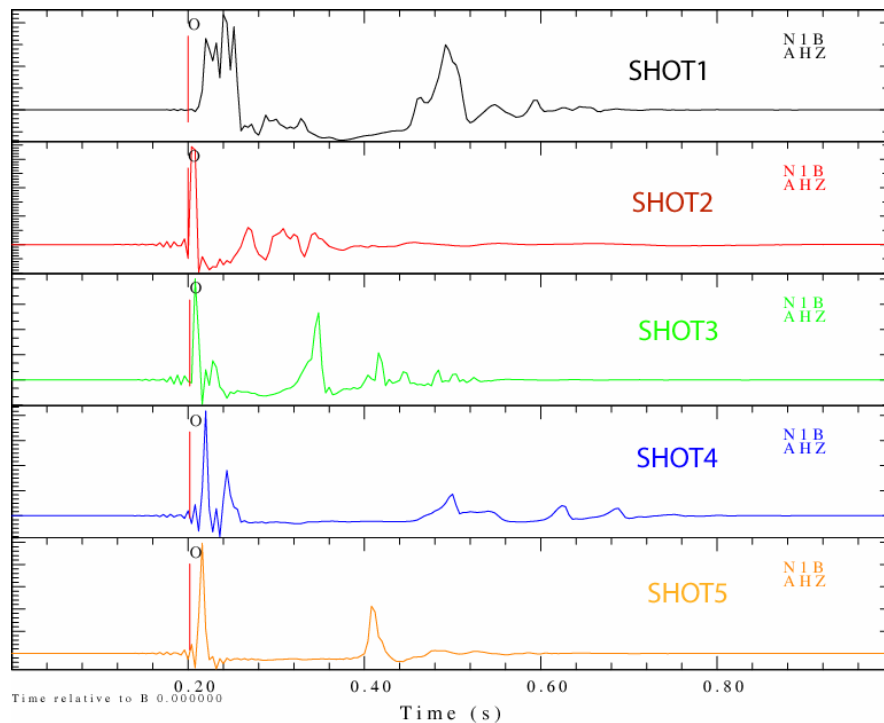


Figure 32. Near-source phenomenology for all five shots recorded on sensor N1B about 5 m from each blasthole collar. These data are not plotted on the same amplitude scales in order to better show the characteristics of the initial shock wave, the -1 g spall, and the spall slapdown(s). Figure 33 provides a better representation of the relative amplitudes between the shots.

Close-in vertical recordings of the shots look remarkably similar, particularly for shots 2, 3, 4, and 5 (Figure 33). Shot 1 appears to have lower frequency energy content in Figure 33. Three component data are shown in Figure 34 for the first three shots. It is interesting to note the large amplitude transverse components at these close-in distances, which has also been observed in prior experiments such as the Frozen Rock Experiment in Alaska.

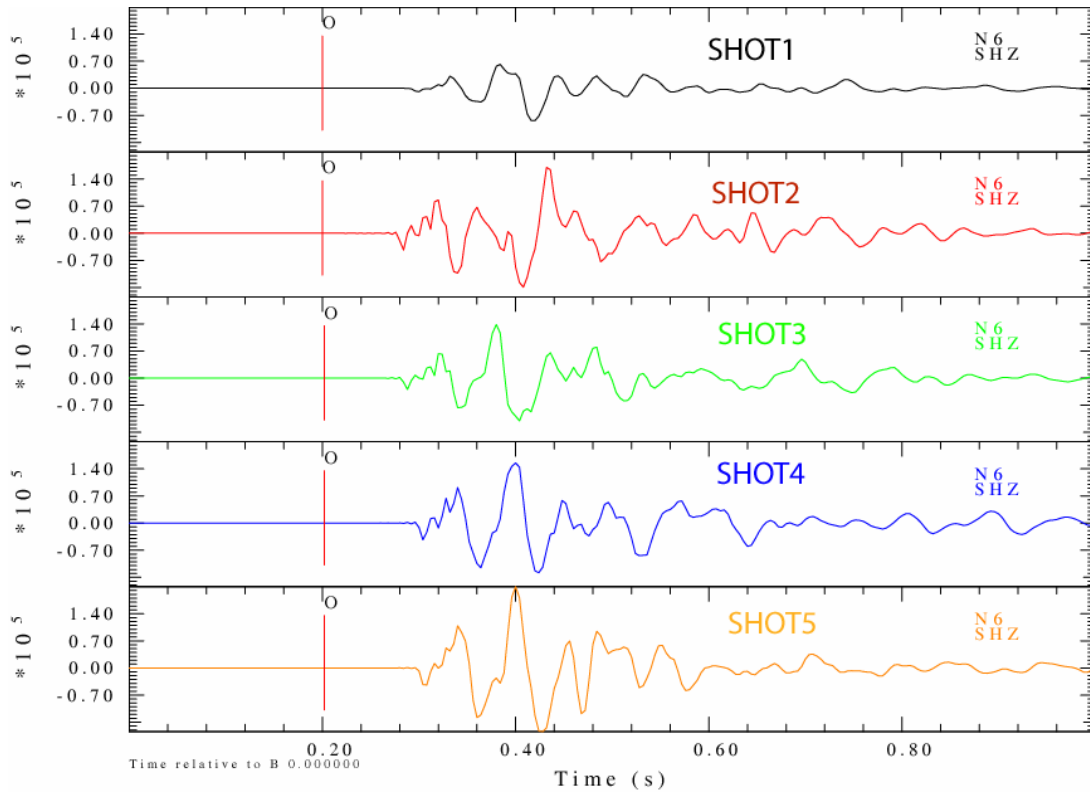


Figure 33. All five shots recorded on the L4-3D vertical channel of station N6. The data were scaled to the maximum amplitude on Shot 5.

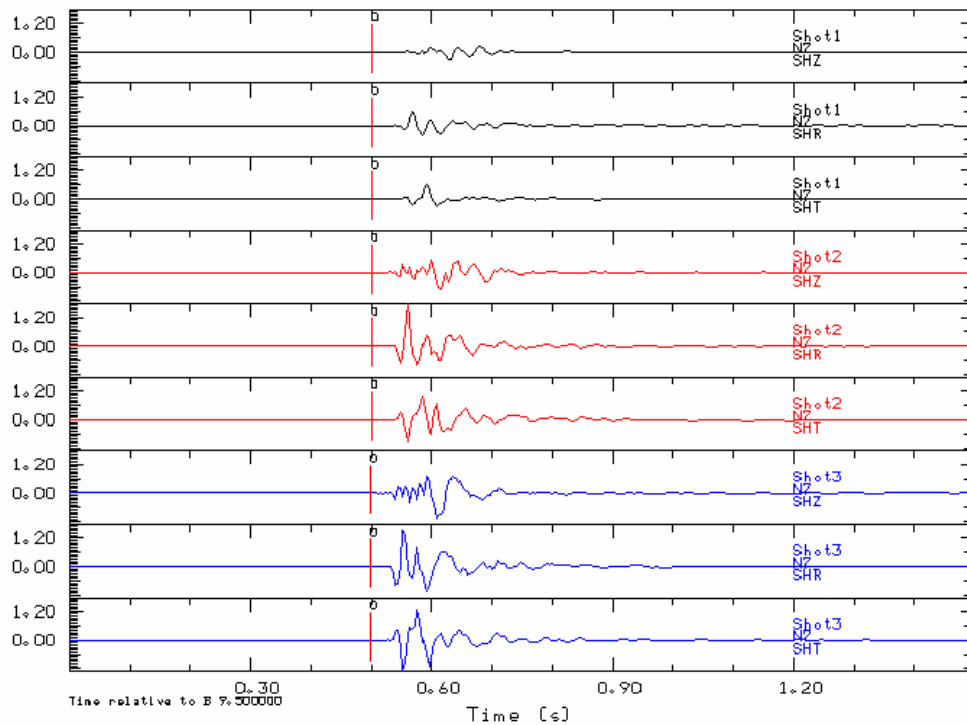


Figure 34. Vertical, radial, and transverse data of shots 1, 2, and 3 recorded on an L4-3D at station N7.

Short Period Linear Arrays

Band-passed, short-period linear array data is presented in Figures 35-37 highlighting the *P*, *S*(?), and surface waves. The pre-event noise data from NE08 (third from the top) is contaminated by the seismic response of a passing automobile.

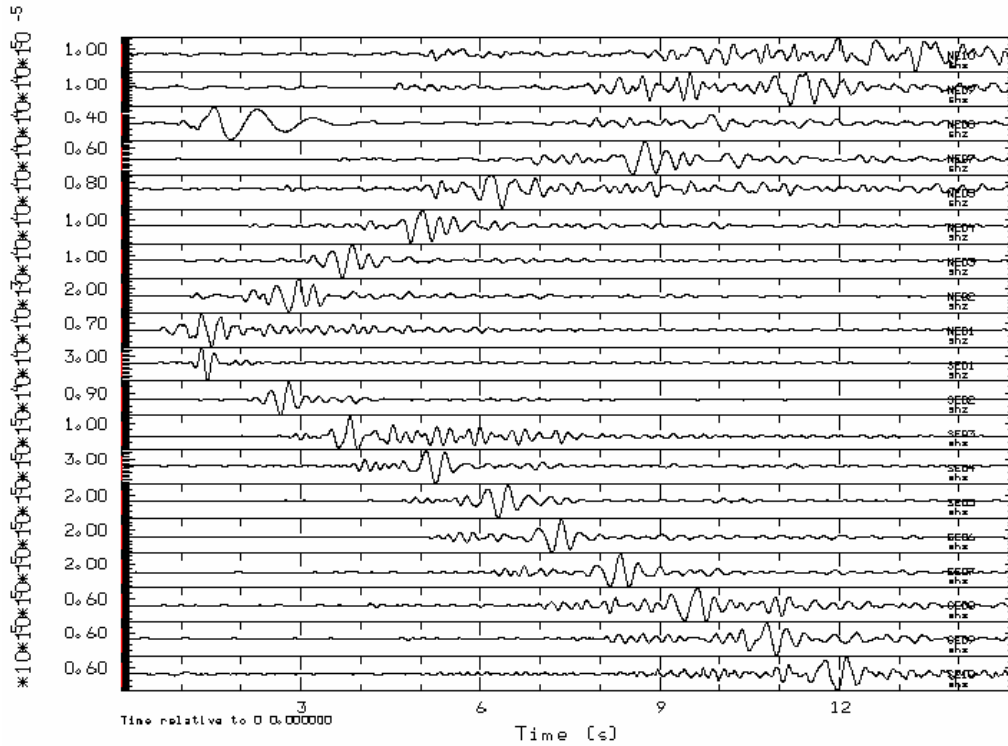


Figure 35. Shot 5 vertical recordings on the short period linear array from north (top) to south (bottom) band passed from 1-4 Hz showing the surface waves.

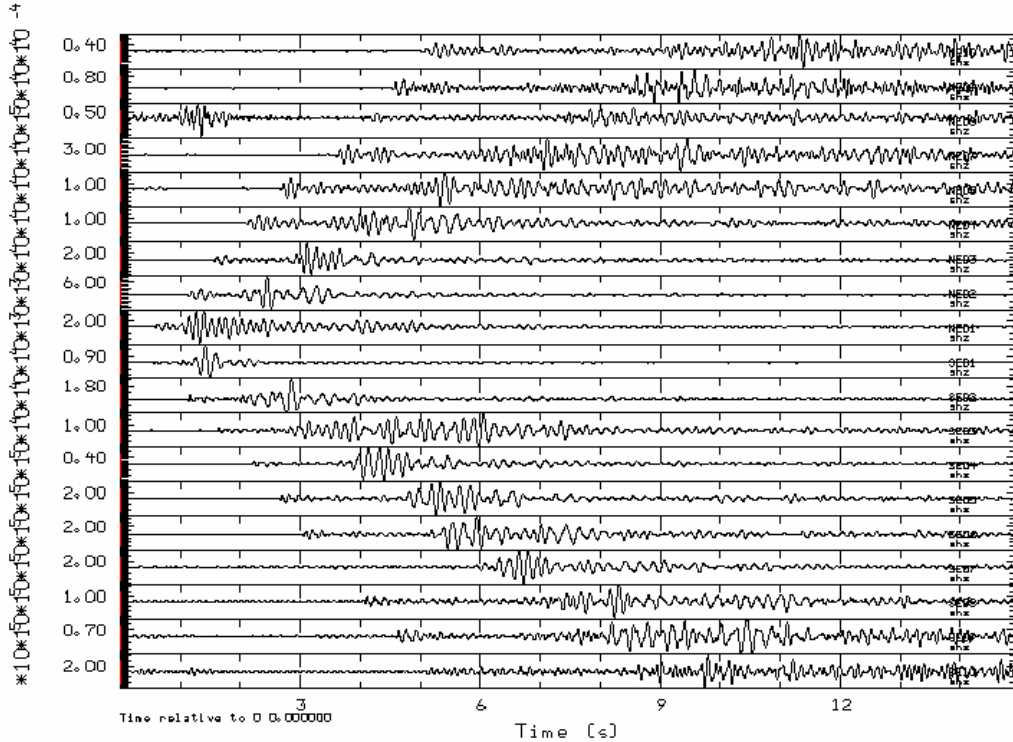


Figure 36. Shot 5 vertical recordings on the short period linear array from north (top) to south (bottom) band passed from 4-10 Hz showing the *P* and *S* (?) waves.

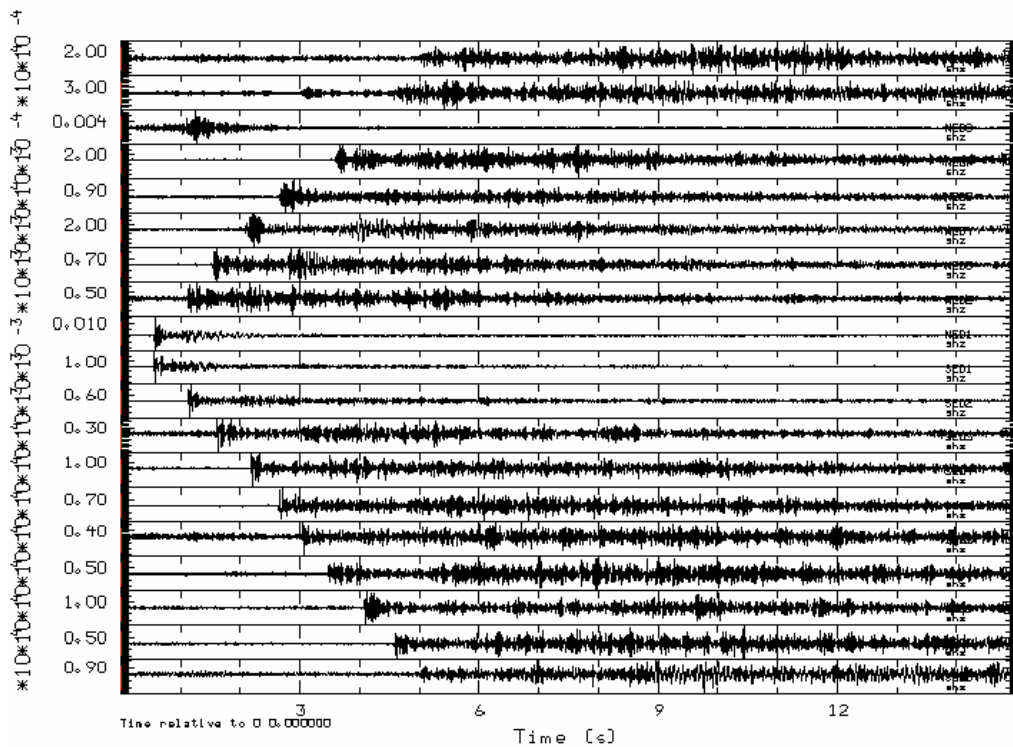


Figure 37. Shot 5 vertical recordings on the short period linear array from north (top) to south (bottom) high passed above 10 Hz showing the *P* waves and *P*- and *S*- coda.

In Figure 38, the Rayleigh waves from the five shots recorded at NE02 are plotted. At this station, the surface wave amplitudes are inversely proportional to the VOD of the explosives. If this trend is observed at other stations, and it is found that the slower VOD explosions generated more damage as the video and surface observations indicate, then these results may suggest that damage around the source is at least partly responsible for the generation of surface waves.

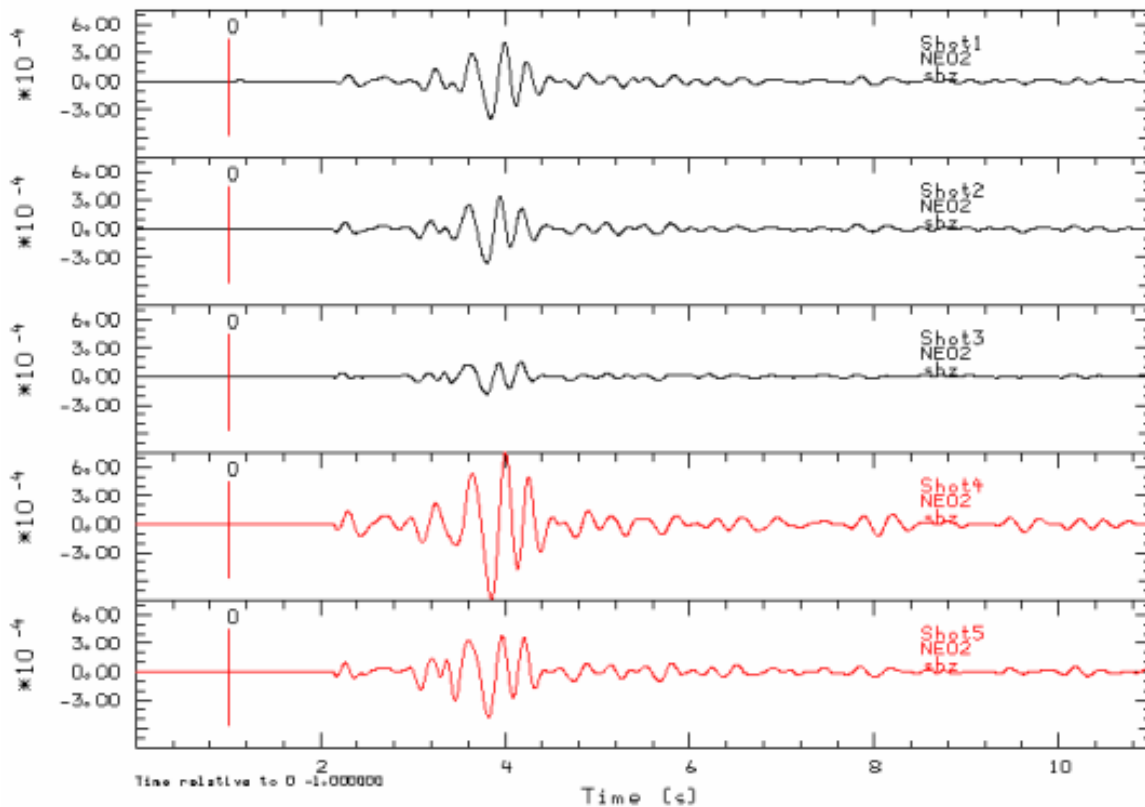


Figure 38. Rayleigh waves at station NE02 for all five shots. Vertical data is band passed between 0.5 and 4 Hz. Note decreasing amplitude of the Rayleigh waves from black powder (Shot 1) to ANFO/Emulsion (shots 2 and 4) to COMP B (shots 3 and 5). The waveforms are color coded by shot size, black=135 lbs, red=270 lbs.

Texans

Data from Shot 5, recorded on the two Texan profiles, are shown in Figure 39 and Figure 40. The data were band pass filtered between 4 and 10 Hz and plotted as a function of distance. The two Texans with either a bad cable connection or geophone are apparent in the plots. *P* and *S* arrivals are obvious in the data. The SE line of Texans appears to have a change in the shear wave arrival times around 13 km distance.

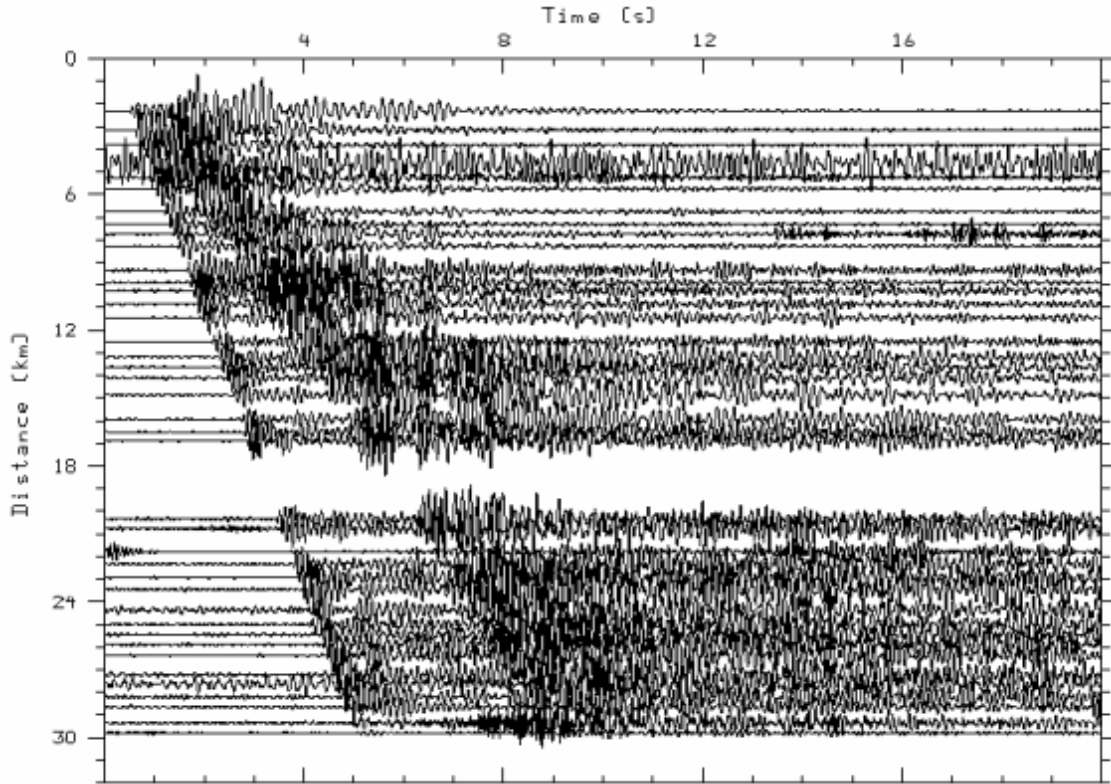


Figure 39. NE Texan line band passed from 4 to 10 Hz.

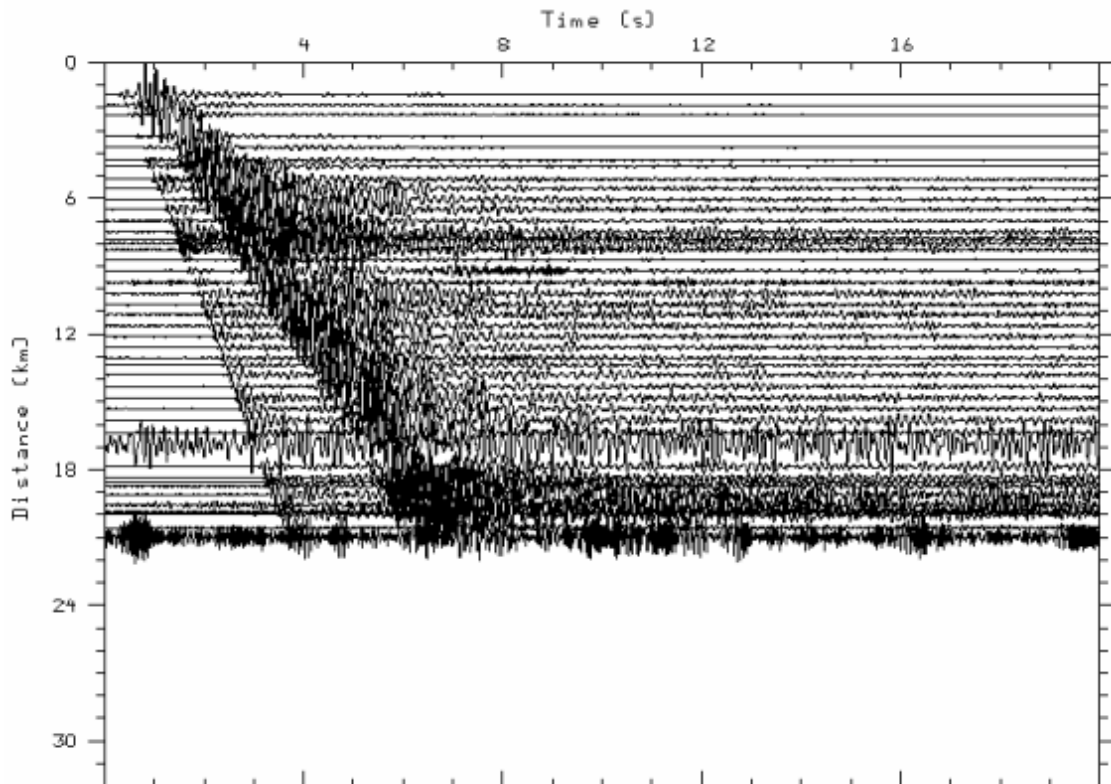


Figure 40. SE Texan line band passed from 4 to 10 Hz.

Regional

A number of regional stations in New England (Figure 41) recorded some or all of the NEDE shots. The signal-to-noise ratio (SNR) varies from fantastic at Lisbon, New Hampshire (LBNH) to not very good at most of the stations for Shots 1-3. With these data, our seismic data recording distance range varies from less than 5 meters (e.g., station N1B) to 281 km (174 miles as recorded at the USGS station in Peaks-Kenny State Park, Maine, PKME). The fact that the *Lg* phase from a 134 lb black powder explosion can be recorded over 280 km from the blast highlights both the low attenuation in New England and the quality of the PKME station. Examples of Love (Figure 42) and Rayleigh (Figure 43) waves from LBNH are plotted along with shots 4 and 5 recorded at PKME (Figure 44).

While the larger shots were recorded on the New England Seismic Network (NESN) stations HNH, QUA2, and FFD, the SNR is very low. HNH seems to be a very noisy station. QUA2 has harmonic noise dominating one of the components. The EHZ-only stations MDV and MIV of the Lamont-Doherty network have adequate SNR. The 3C station FRNY is probably the second-best recording (after LBNH) of the events from these permanent stations.

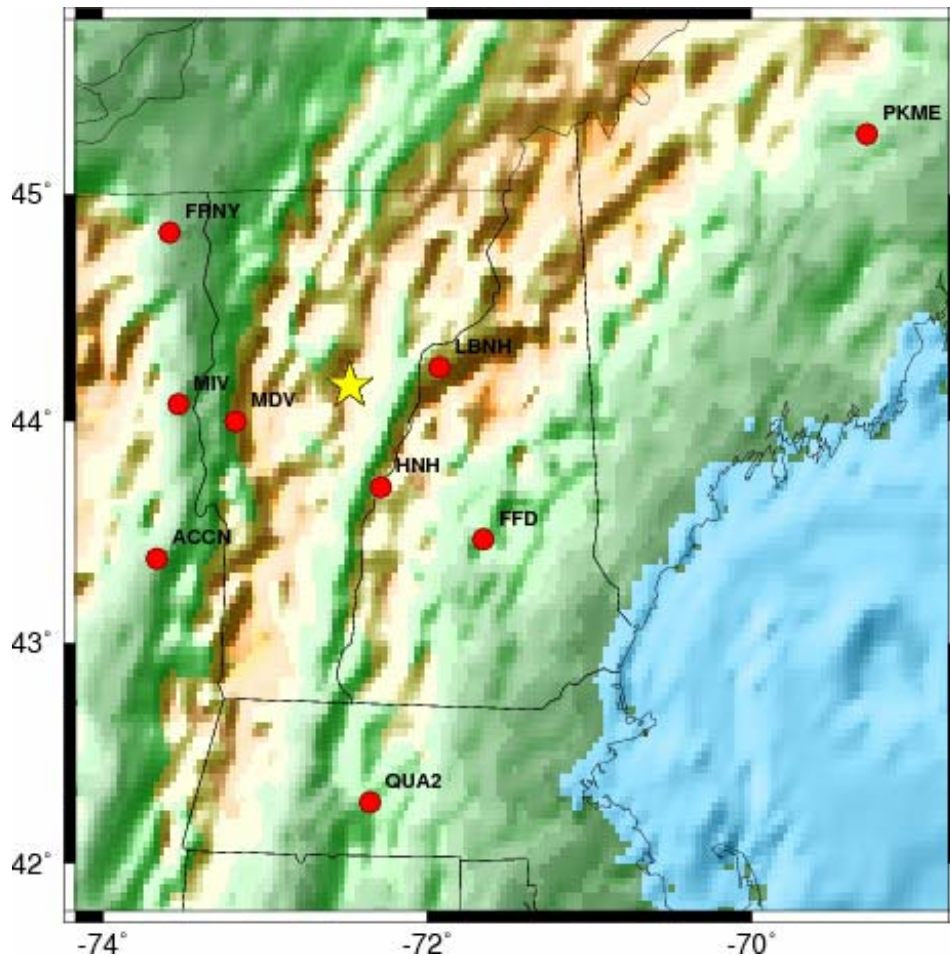


Figure 41. Seismic stations in New England that recorded some of the NEDE blasts (star).

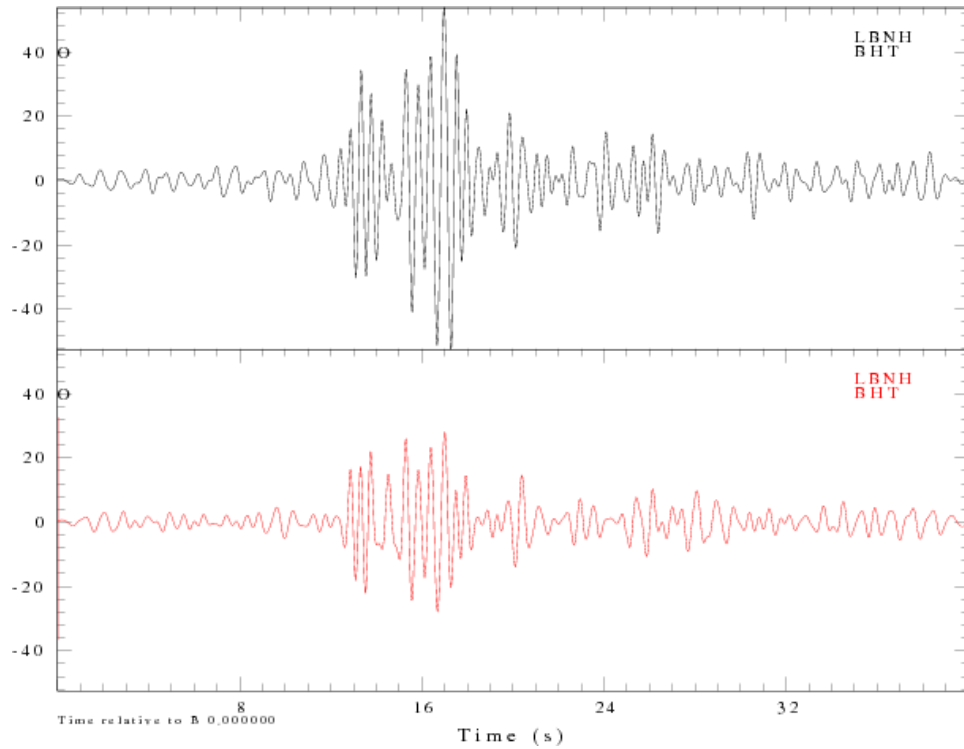


Figure 42. Love waves recorded on the BHT component of LBNH for Shot 4 (black) and Shot 5 (red). The later part of the wave train may be Rayleigh-waves that have scattered onto the transverse components. However, the first part of the wave train is definitely SH motion.

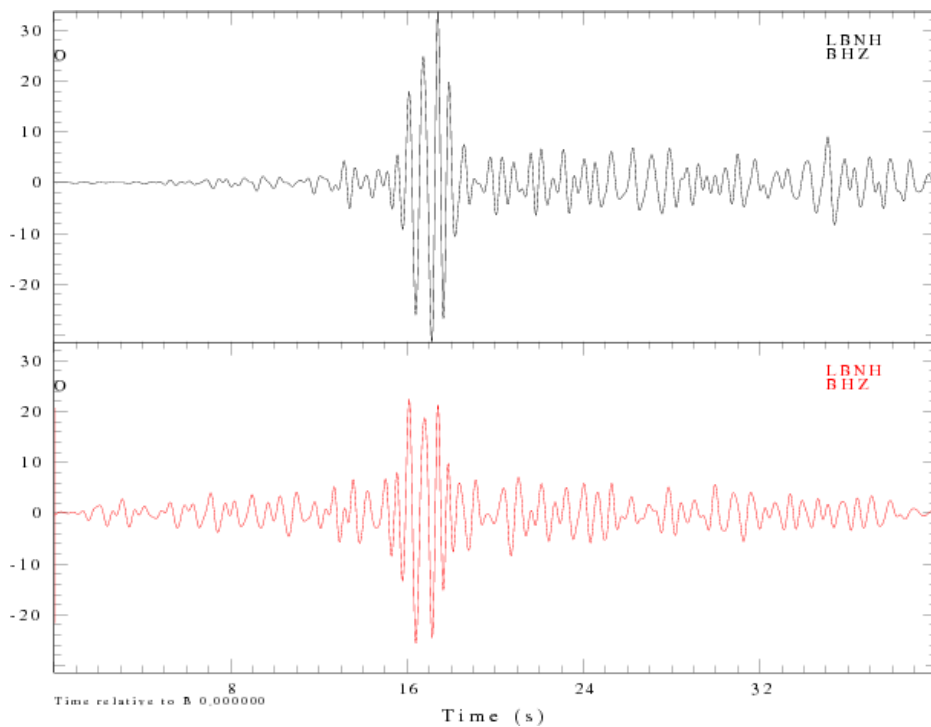


Figure 43. Rayleigh-waves recorded on the BHZ component at LBNH from Shots 4 (black) and 5 (red).

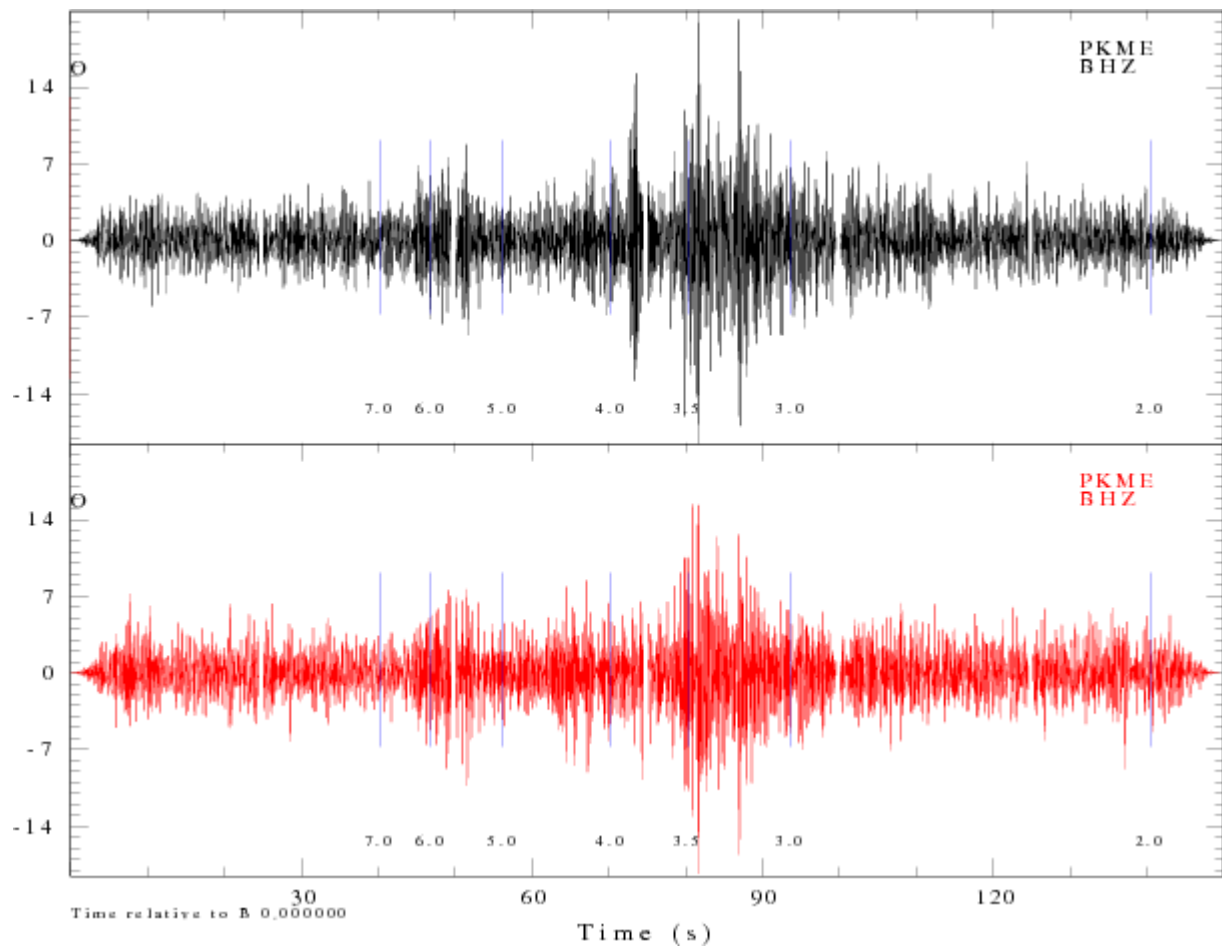


Figure 44. Shots 4 (black) and 5 (red) recorded at PKME (280 km). Note the impulsive arrival at group velocity 4 km/s only on the Shot 4 record.

CHAPTER 5. PRE- AND POST-BLAST SOURCE ROCK CHARACTERIZATION

To quantitatively and qualitatively measure the damage caused by the blasts, geophysical studies were conducted on the source rock before and after (currently on-going) the explosions. Figure 45 shows initial planning for examining the damage to the source rock by drilling observational boreholes near the planned explosion. The pre-existing fractures and rock properties could be measured before the blast and then the fractures and damage could be observed in the boreholes after the explosions. This plan was modified for the actual experiment in that 2" diameter core was drilled near the explosion borehole and two boreholes were drilled on either side of the explosion borehole to perform a cross-hole tomography (Figure 46).

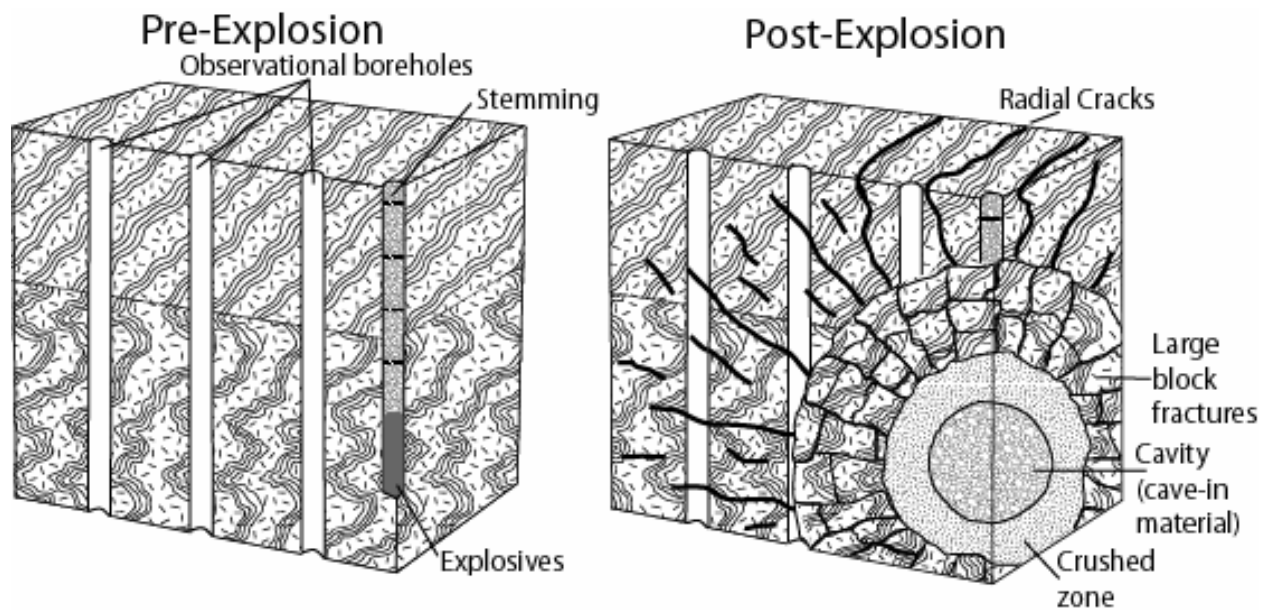


Figure 45. Diagram showing the initial planning for geophysical logging of the source rock before and after the explosions.

Core Samples

A photo of core taken from the test site is shown in Figure 47. The driller, Mike McGinley, had to break much of the core from the bottom of the hole due to the lack of natural fractures in the granite. Post-blast core samples are currently being extracted to compare to the pre-blast samples.

A velocity analysis of the core extracted from near Shot 2 was completed by Peter Boyd (New England Research, Inc). Figure 48 plots the compressional wave velocity as a function of depth in the core hole. The velocity increases with depth and has a change in slope at approximately 30 feet. The increase in compressional wave velocity with orientation, at a single depth, can approach 25 percent.

Figure 49 shows the diametrically-transmitted compressional wave velocity, as a function of chord orientation, in the core specimen recovered from near Shot 2. The “Fast” chord defines the strike of the rift plane in the Barre granite, which is N30E° at this site (Donald Murray, pers. comm. 2008). The rift plane is considered to be near-vertical and is the orientation that the granite blocks break cleanly when being quarried. The fastest compressional wave velocity is ~19 percent greater than the slowest velocity in this specimen.

Televiewer

Dorothy Richter, Rob Garfield, and Alexis Martinez of Hager-Richter Geoscience were responsible for performing optical and acoustic televiewer logging of the test site (Figure 50) before and after the blasts. The resulting images provide a 360° view of the borehole walls for mapping of fractures (Figure 51). Table 12 lists the fractures found in core hole 1 (CH-1), and the rank defines the size and aperture of the fracture. This examination was carried out for all five core holes and will be conducted again after the explosions to determine the damage done to the granite by the blasting (assuming borehole stability).

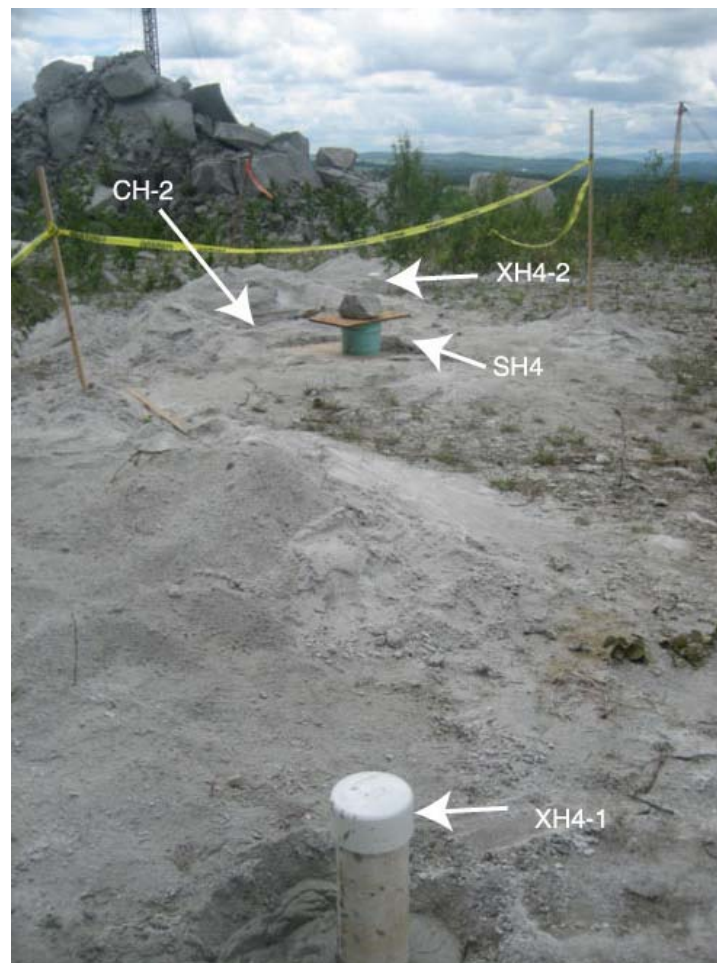


Figure 46. Typical layout of blast hole (SH4), core hole (CH-2), and cross-hole tomography holes (XH4-1 and XH4-2) for all five shots.



Figure 47. Example of unfractured core taken from the test site.

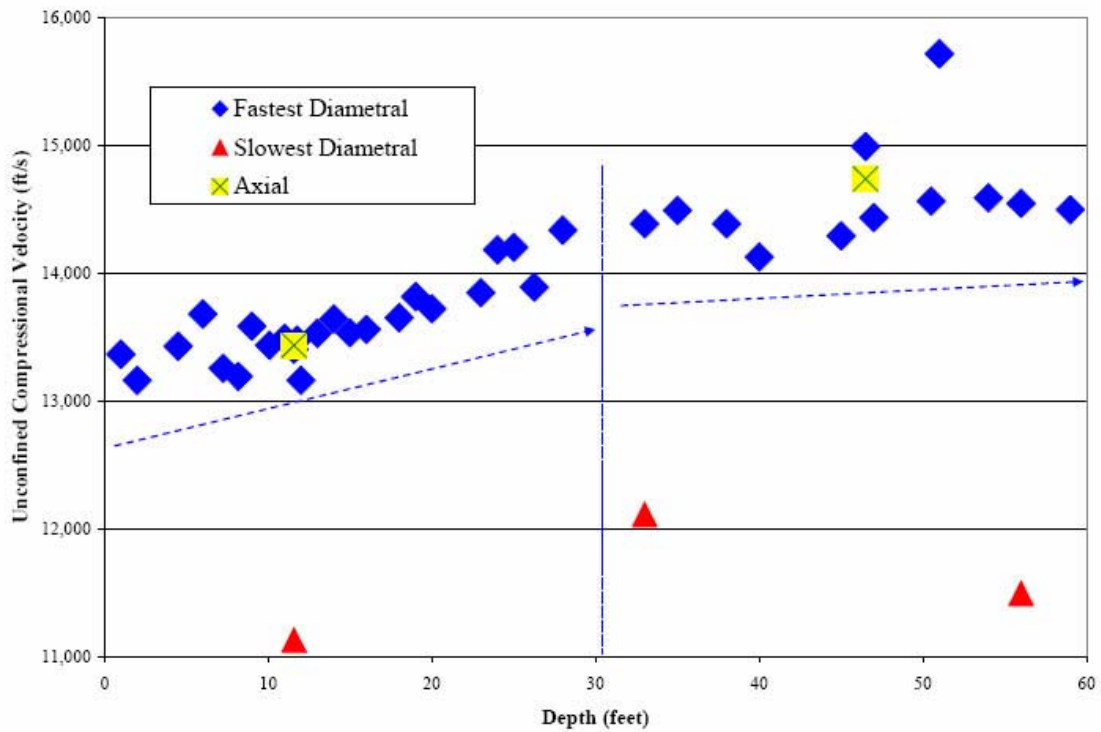


Figure 48. Compressional wave velocity determined in laboratory study of core taken from near Shot 2. The diametrals indicate orientation in the core hole.

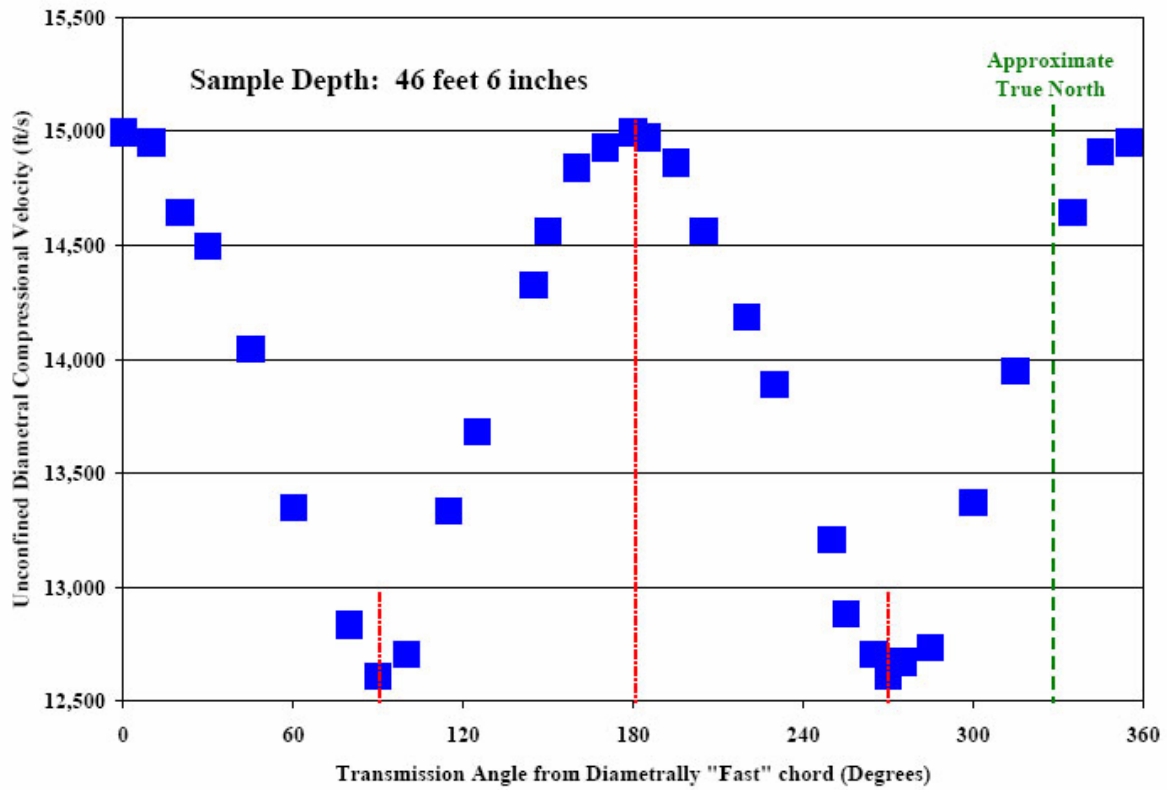


Figure 49. Compressional wave velocity as a function of azimuth in the Barre granite near Shot 2. The fast direction is oriented $\sim 30^\circ$ east of true north and is believed to follow the “rift” of the granite.



Figure 50. Logging with acoustic and/or optical televiewer.

Table 12. Structures in the Granite of Core Hole 1.

Depth (ft)	Dip Azimuth (°)	Dip Angle (°)	Bedrock Structure
6.5	187	82	Fracture Rank 1
7.7	101	4	Fracture Rank 3
8.3	185	17	Fracture Rank 2
8.4	265	14	Fracture Rank 2
8.5	263	19	Fracture Rank 2
9.9	179	67	Fracture Rank 1
10.1	195	7	Fracture Rank 2
10.2	172	20	Fracture Rank 2
11.9	82	41	Fracture Rank 1
11.9	260	16	Fracture Rank 2
13.2	353	45	Fracture Rank 1
13.6	224	39	Fracture Rank 2
14.6	65	48	Fracture Rank 2
21.1	241	68	Fracture Rank 2
39.6	105	26	Fracture Rank 2
50.8	105	26	Fracture Rank 2

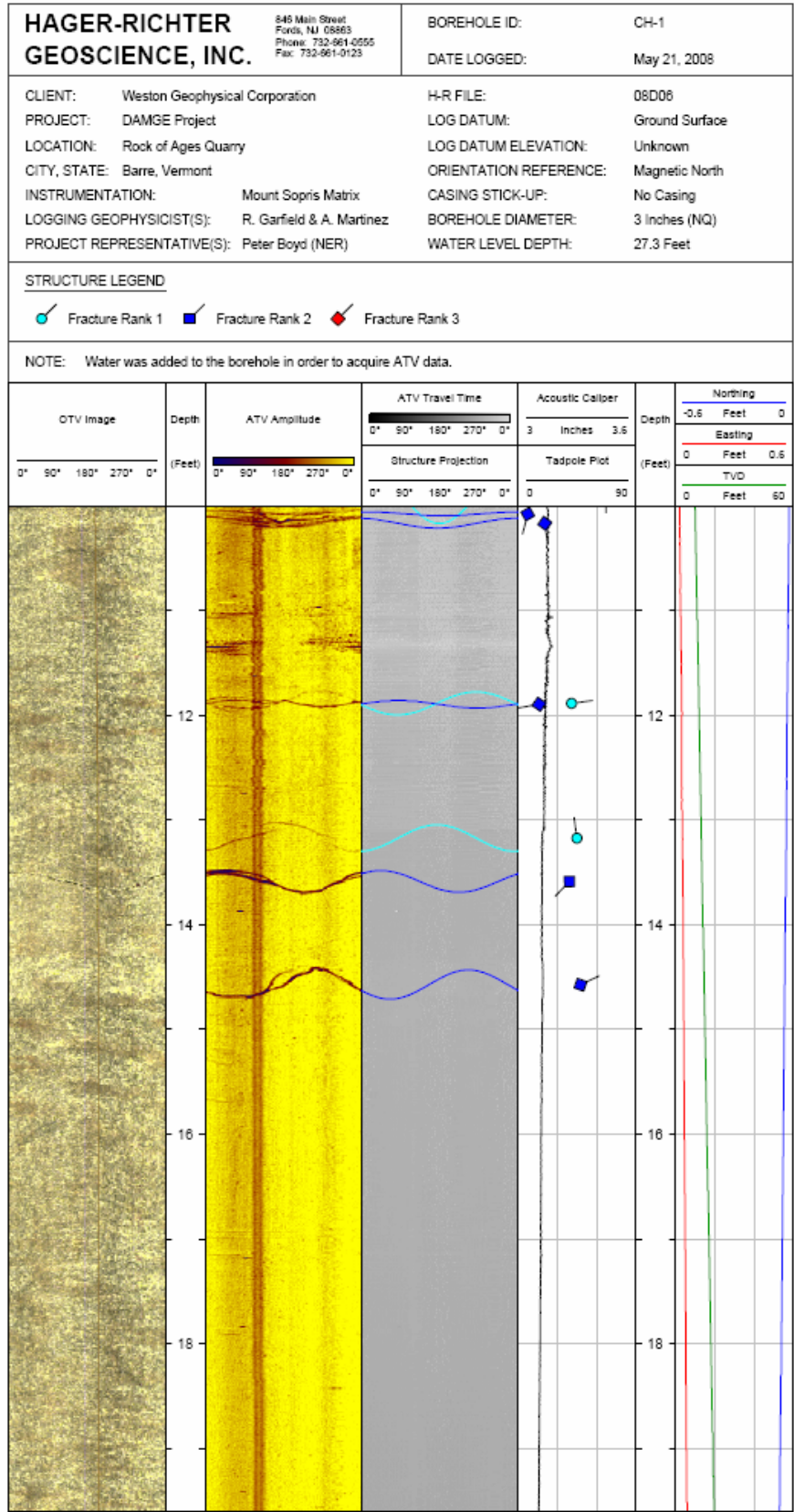


Figure 51. Optical and acoustic televiewer log documenting fractures in the granite.

Cross-hole Tomography

A cross-hole tomography was to be conducted prior to the blasting across each blast hole, but the grout used to hold the PVC pipe in the holes was bentonite-based instead of cement based. The result is shown in Figure 52. The grout did not solidify properly to secure the PVC pipe and “attach” it to the bore hole wall. It was therefore not possible to conduct the cross-hole tomography. New holes are being drilled after the blasting and will be grouted properly so the tomography can be conducted. The tomography will highlight the region with seismic velocities that are decreased from the background level and therefore have sustained damage and fracturing during the blasting. Jeff Reid of Hager-Richter Geoscience will be responsible for conducting this study.



Figure 52. Grout collapsed around PVC pipe in a cross-hole tomography bore hole.

CHAPTER 6. ACKNOWLEDGMENTS

We wish to thank the Air Force Research Laboratory for funding the experiment and Rock of Ages for allowing us to blast their beautiful granite rock. We express our sincere appreciation to The Hollow Inn in Barre, VT for putting up with our equipment for a week, as well as the helpful Vermont residents who let us put seismometers on their property and the towns in Vermont that gave permission for seismometer installation. We also thank Johnson Artesian for their help on the project. Finally, we thank Lynne Murray and family for a wonderful dinner and evening.

CHAPTER 7. REFERENCES

- Ashby, M.F. and C. G. Sammis, (1990). The Damage Mechanics of Brittle Solids in Compressions. *Pure appl. Geophys.* **133**. 489-521.
- Doolan, B., (1996). The Geology of Vermont, *Rocks and Minerals Magazine*, Vol. 71, No. 4, pp. 218-225.
- Melosh, H. J., (1979). Acoustic Fluidization: A New Geologic Process. *J. Geophys. Res.*, **84**, 7513-7520.
- Patton, H. J. and S. R. Taylor, (1995). Analysis of *Lg* Spectral Ratios from NTS Explosions: Implications for the Source Mechanism of Spall and the Generation of *Lg* Waves, *Bull. Seism. Soc. Am.* **85**, 220 - 236.
- Patton, H., J. Bonner, and I. Gupta, (2005). *Rg* Excitation by Underground Explosions: Insights from Source Modeling the 1997 Kazakhstan Depth of Burial Experiments. *Geophys. J. Int.* doi:10.1111/j.1365-246X.2005.02752.x.
- Rodean, H.C., (1971). Nuclear-Explosion Seismology, U. S. Atomic Energy Commission, TID-25572, 156 pp.
- Sammis, C. G. (2002). Generation of High-Frequency *P* and *S* Wave Energy by Rock Fracture During a Buried Explosion: Its Effect on *P/S* Discriminants at Low Magnitude, Proceedings of the 24th Seismic Research Review – Nuclear Explosion Monitoring: Innovation and Integration, Sept. 17-19, 2002, Ponte Verde Beach, Florida, 542-551.
- Stevens, J.L., G. E. Baker, H. Xu, T.J. Bennett, N. Rimer, and S.M. Day, (2003a). The Physical Basis of *Lg* Generation by Explosion Sources. *Proceedings of the 25th Annual Seismic Research Review on Nuclear Monitoring Technologies*, Tucson AZ
- Stevens, J.L., N. Rimer, H. Xu, G.E. Baker, S.M. Day, (2003b). Near-field and Regional Modeling of Explosions at the Degelen Test Site. SAIC Final Report SAIC-02/2050.

APPENDIX A. HUDDLE TEST

We conducted a huddle test with all the near-source and linear short period array sensors in Lexington, MA on 6 July 2008 prior to packing the equipment up and trucking it to Barre, VT. The two primary goals of this test were to assemble working stations with DAS, GPS clocks, hard drives, and sensors and to record the same signals on all the sensors so we can compare instrument response for correcting the NEDE blast data.

Figure 53 shows the Weston, PASSCAL, and LANL sensors with batteries and digitizers in close proximity to record the same signals at 250 sps. Table 13 lists the equipment used during the huddle test. The PASSCAL and LANL sensors did not have feet so it was a challenge to level them on the sloping parking lot.



Figure 53. Huddle test in the Weston Geophysical parking lot prior to the experiment.

Some of the old LANL sensors had bad channels and were not used for the actual experiment. For the short period equipment, a Weston RT130 power cable was found to have reversed polarity connectors. Reversing the connection to the battery fixed this problem. In addition, the parameter files did not upload properly to two DAS and the data was set to be dumped to disk and ethernet. This caused the internal memory to fill and dump to disk once and then stop recording. Data was collected for the majority of the huddle test though. A PASSCAL RT130

would not boot so no data was collected. This DAS was repaired in the field and used for the experiment. We also found that leaving the new RT130 Palm controllers in the sun causes the screen and system to act erratically.

Table 13. Huddle Test Setup.

DAS	Disk	GPS	CH 1-3	CH 4-6	Notes
734	5715	663	Endevco 6	Endevco 2	All chans good
619	87	664	L4-3D 619	TerraTek 9	All chans good (TT hi-freq noise on Z and E)
716	5106	248	L4-3D 84	TerraTek 13	L4 bad E; TT has bad N
745	5236	299	L4-3D 37	TerraTek ??	Re-do test
739	5237	674	L4-3D 623	TerraTek 6	L4 bad E and N valid >30 Hz; TT good, Z may be enhanced
737	5180	670	L4-3D 189	TerraTek 4	Re-do test
744 (1768)	5713	244	L4-3D 257	TerraTek 7	Re-do test
733	5959	669	L4-3D 628		All chans good
9E4B	-	2514	L4-3D L41167		Good
9D8F	-	2661	L4-3D L41166		Good; 1 data dump
9DEA	-	2448	L4-3D L41169		Good
9E18	-	2565	L4-3D L41162		Good
9E1B	-	2711	L4-3D L41164		Good; 1 data dump
9D63	-	2665	L4-3D L41168		Good
9E42	-	2516	L4-3D L41161		Good
9E4F	-	2531	L4-3D L41165		Good
9DAA	-	2520	L4-3D L41170		Good
9E17	-	2809	L4-3D L41163		Good
939E	-	4194	L22 449L		Good
930E	-	3890	L22 643L		Good
9E45	-	4175	L22 642L		Good
9E40	-	4161	L22 468L		DAS would not boot; not tested
A198	-	4176	L22 462L		Good
9E50	-	4188	L22 720L		Good
940F	-	4196	L22 479L		Good
9312	-	4189	L22 496L		Good
9D42	-	4198	L22 494L		Good
9669	-	4179	L22 459L		Good

Data examples from the huddle test are shown in the following figures. The “flip test” (Figure 54 and Figure 55) for accelerometers involves turning the accelerometer upside down for a moment to record 1 g of acceleration. For the seismometers, various signals are examined to determine if all channels are working and how the signals vary from sensor to sensor (Figure 56, Figure 57, and Figure 58). Both the Weston L4-3D (Figure 59) and the PASSCAL L22 (Figure 60) sensors have self-similar responses. It is important to understand the response difference between the L4-3D and L22 sensors. Figure 61 compares the same vertical signal on the two types of sensor after the data has been converted to velocity (cm/s). The signals are almost identical. The polarity on the Weston L4-3D horizontal components needs to be reversed, but almost identical signals were produced for these components after correction as well.

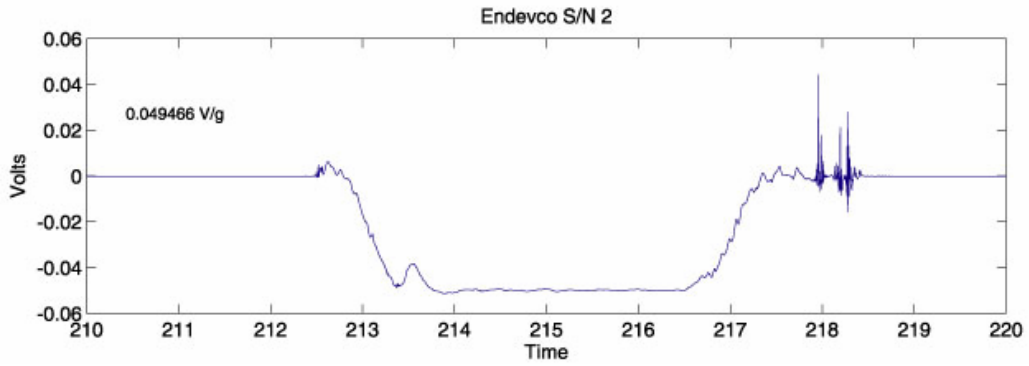
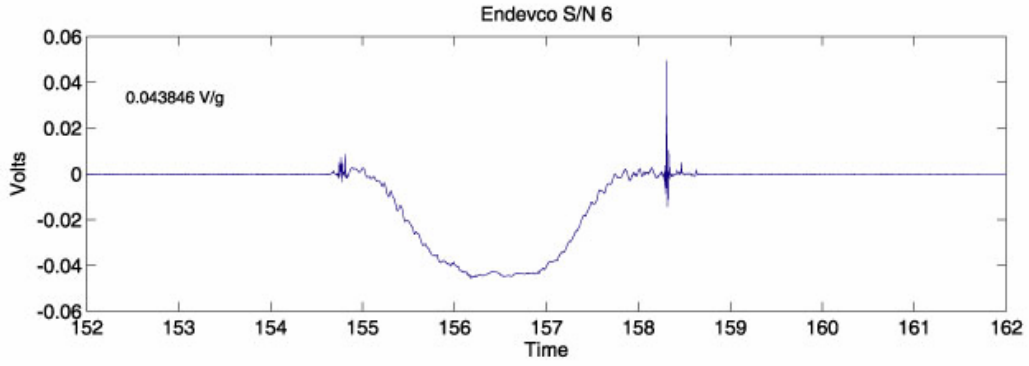


Figure 54. "Flip test" for Endeveco sensors.

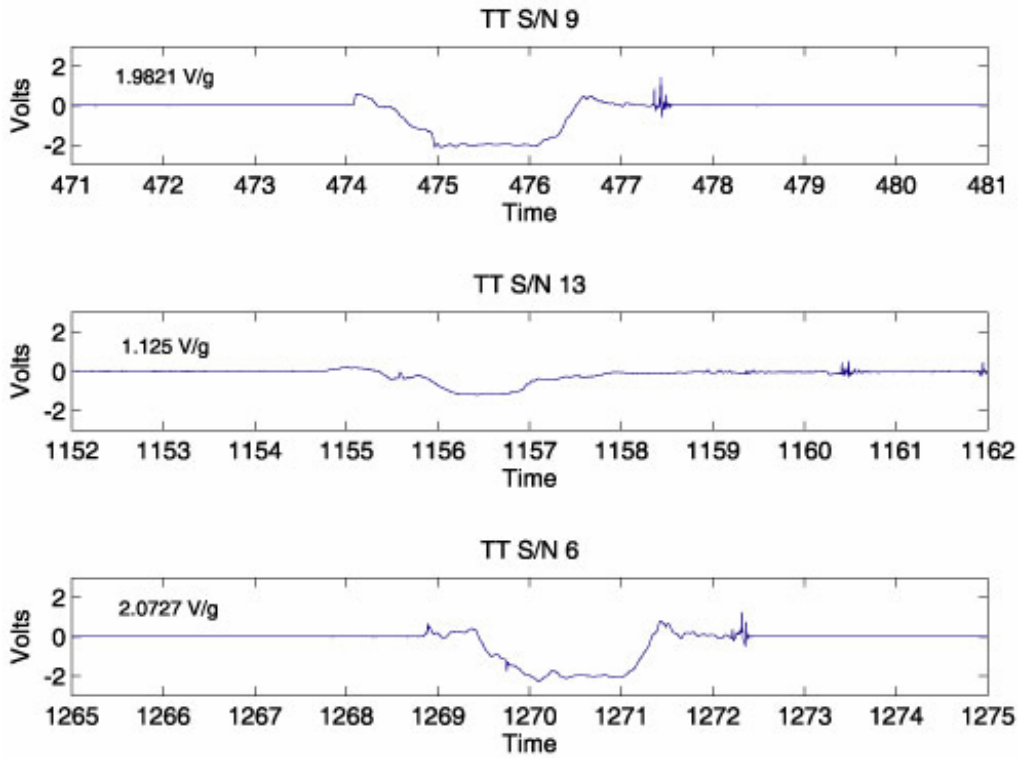


Figure 55. "Flip test" for TerraTek sensors.

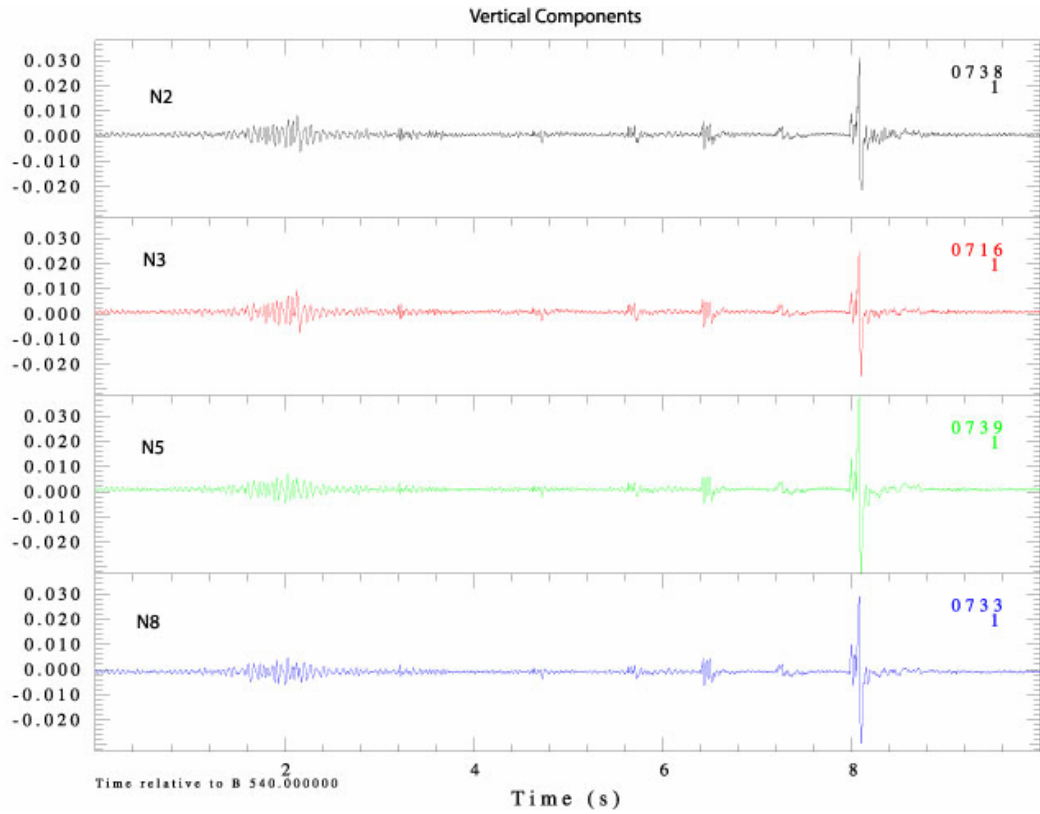


Figure 56. Near-source vertical L4-3D components.

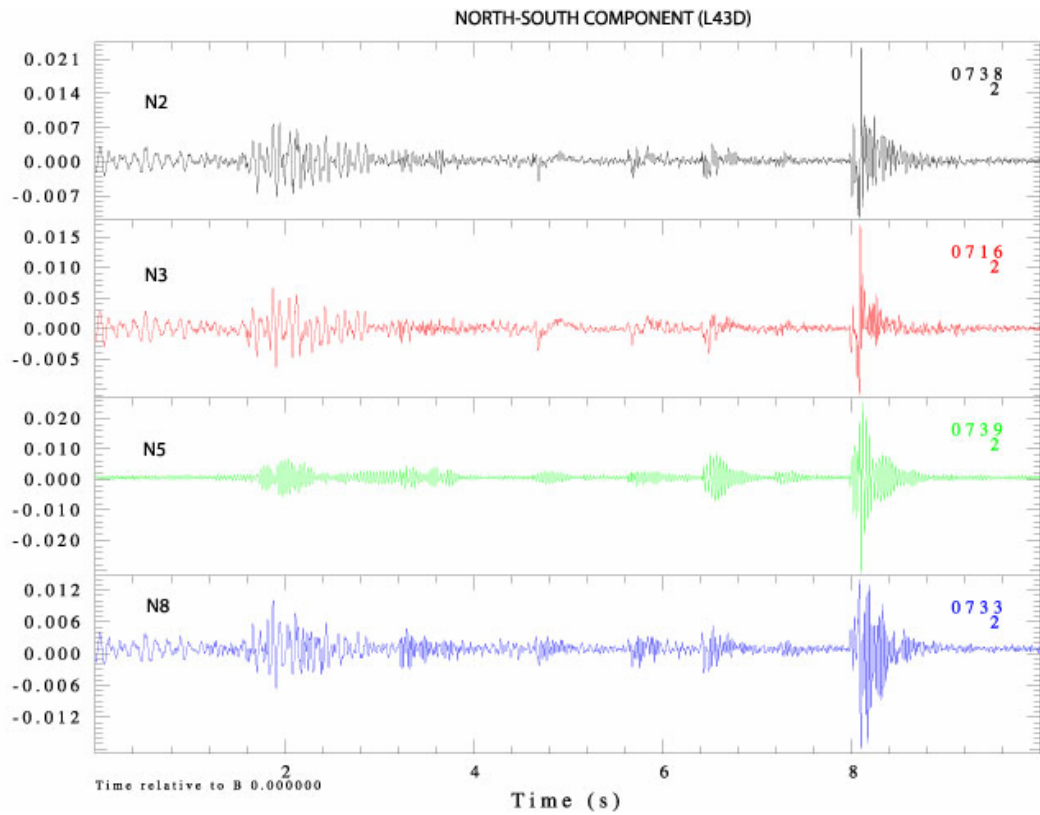


Figure 57. Near-source north/south L4-3D components.

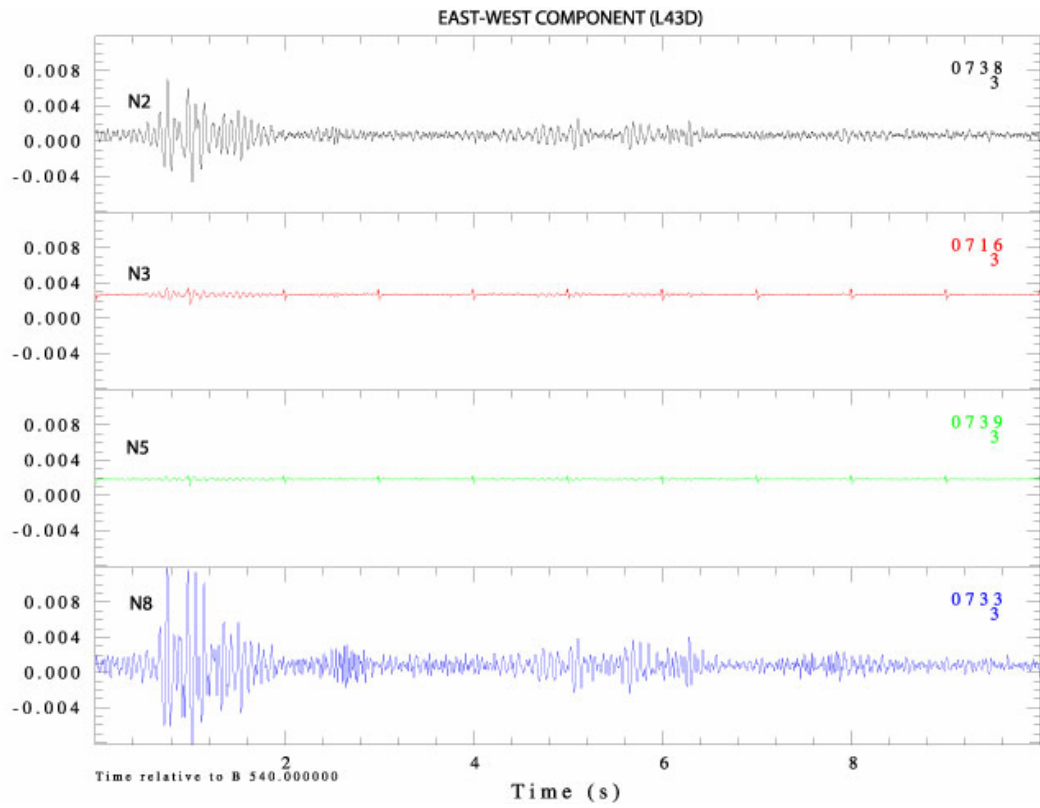


Figure 58. Near-source east/west L4-3D components.

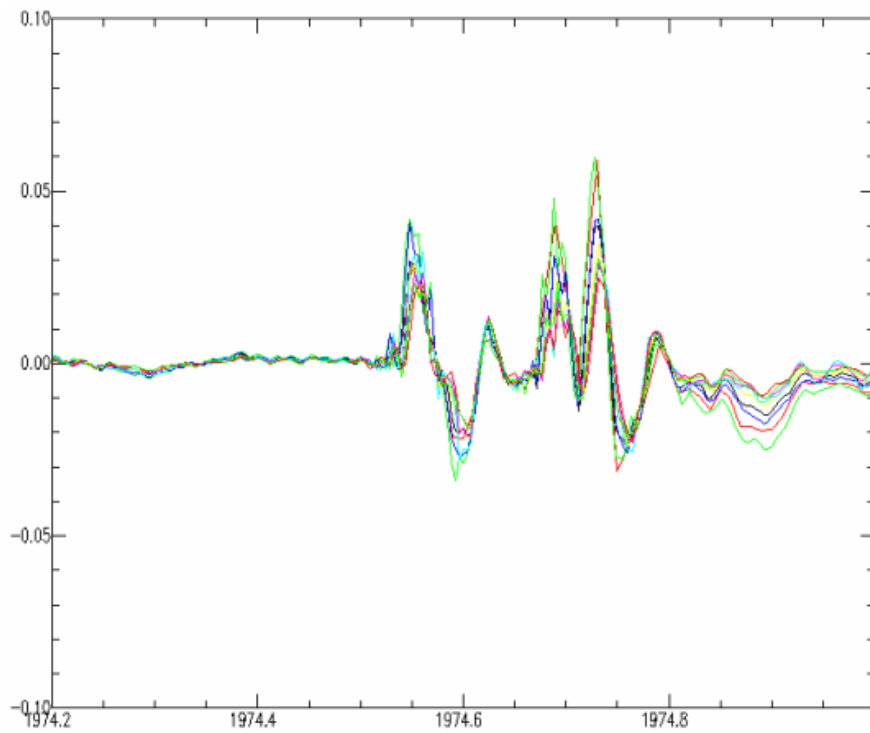


Figure 59. Weston L4-3D vertical component huddle data for all sensors.

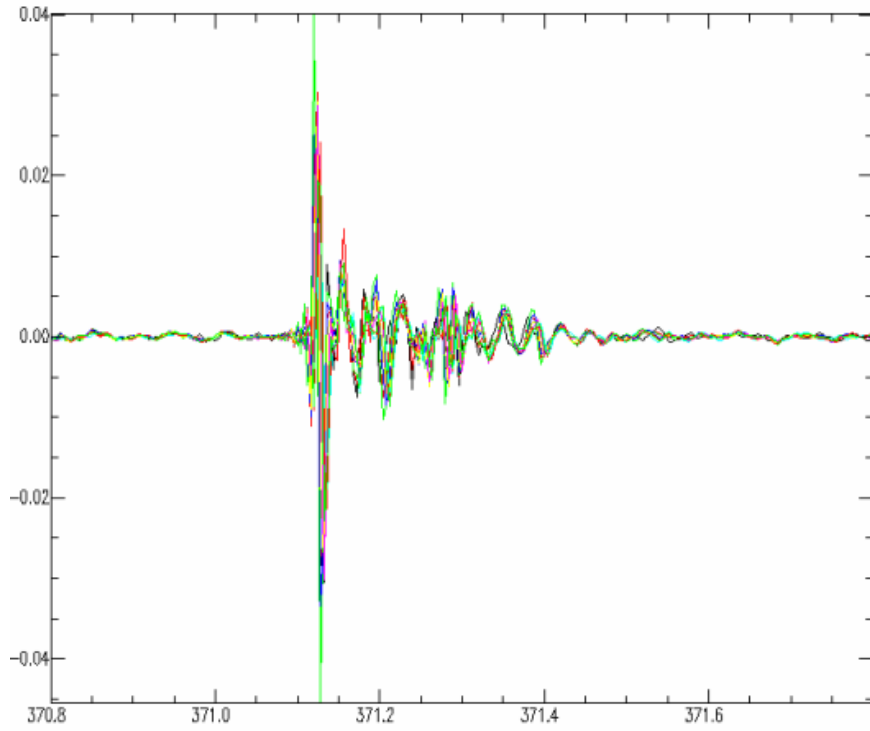


Figure 60. PASSCAL L22 vertical component huddle data for all sensors.

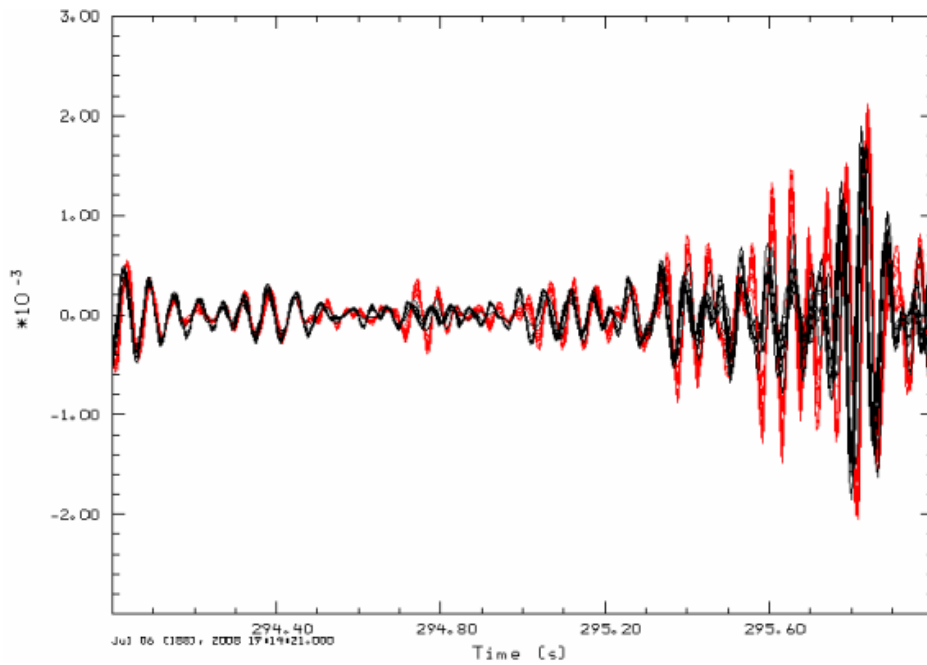


Figure 61. Comparison of Weston L4-3D (red) and PASSCAL L22 (black) vertical huddle data between 2 and 20 Hz after converting all data to velocity (cm/s).

APPENDIX B. L22 IN-SITU RESPONSE

Serial #	Channel	String	Frequency	Damping	Resistance	Sensitivity (V/cm/s)	Impedance	LoDrv Impedance	Distortion	Polarity	Leakage	GeoType
449L	1	Single	2.11	0.7	4501	0.893	5012.4	5017	0.05	0	0	L-22D-200804
449L	2	Single	2.07	0.728	4447	0.859	4989.2	4994	0	0	0	L-22D-200804
449L	3	Single	2.01	0.75	4442.6	0.935	4997.8	5002	0.17	0	0	L-22D-200804
459L	1	Single	2.17	0.765	4281	0.934	4927.1	4947	0.01	0	0	L-22D-200804
459L	2	Single	1.88	0.812	4300.9	0.872	4791.2	4795	0.12	0	0	L-22D-200804
459L	3	Single	2.1	0.702	4287.9	0.878	4787.9	4792	0.04	0	0	L-22D-200804
462L	1	Single	2.05	0.762	4344.1	0.919	4970.6	4975	0.08	0	0	L-22D-200804
462L	2	Single	2.07	0.785	4392	0.9	5045	5049	0.14	0	0	L-22D-200804
462L	3	Single	2.09	0.818	4403.9	0.989	5145.1	5150	0.14	0	0	L-22D-200804
479L	1	Single	2.23	0.633	4369.8	0.959	4946.2	4957	0.12	0	0	L-22D-200804
479L	2	Single	1.99	0.697	4258.8	0.806	4885.8	4894	0.55	0	0	L-22D-200804
479L	3	Single	1.97	0.804	4269.5	0.917	4884.3	4890	0.03	0	0	L-22D-200804
494L	1	Single	1.99	0.773	4532.2	0.906	5101.2	5105	0	0	0	L-22D-200804
494L	2	Single	2	0.752	4574	0.866	5074.8	5079	0	0	0	L-22D-200804
494L	3	Single	2.04	0.769	4489.7	0.938	5050.9	5056	0.23	0	0	L-22D-200804
496L	1	Single	1.96	0.745	4536	0.917	5026.7	5031	0.72	0	0	L-22D-200804
496L	2	Single	-5.11	0.431	4470.6	1.194	4993.7	4998	0.03	0	0	L-22D-200804
496L	3	Single	2.01	0.727	4559.5	0.893	5058.5	5063	0.04	0	0	L-22D-200804
642L	1	Single	2.03	0.808	4465.7	0.99	5194.8	5199	0.36	0	0	L-22D-200804
642L	2	Single	2.02	0.818	4487.1	0.953	5161.3	5166	0.03	0	0	L-22D-200804
642L	3	Single	1.85	0.826	4340	0.844	4817.4	4822	0	0	0	L-22D-200804
643L	1	Single	2.13	0.733	4298.9	0.929	4919.5	4924	0	0	0	L-22D-200804
643L	2	Single	2.07	0.742	4169.7	0.915	4728.3	4733	0.18	0	0	L-22D-200804
643L	3	Single	2.5	0.623	4387.7	1.041	5073.2	5078	0.44	0	0	L-22D-200804
720L	1	Single	2.13	0.607	4434.1	0.89	4863.5	4869	0.33	0	0	L-22D-200804
720L	2	Single	2.32	0.683	4534.2	0.916	5188.1	5193	0.2	0	0	L-22D-200804
720L	3	Single	2.03	0.707	4299.3	0.939	4954.6	4960	0.46	0	0	L-22D-200804

*Note: For sensor 462L, channels 2 and 3 were swapped. This table reflects data as collected in the field and has not been modified to fix that problem.

APPENDIX C. L4-3D FACTORY REPSONSE

1. **General**
 - a) Serial Number: L41161
 - b) Tested at 78 ° F
 - c) Leakage to case >100 Megohms at 500 volts.

2. **Calibration Coils, In Series**
 - a) Resistance: 21.3 Ohms
 - b) Polarity: Negative voltage at socket A with respect to socket B when suspended mass moves toward to the case bottom

3. **Signal Coil (Vertical Detector)** Serial Number: L41171
 - a) Electrodynamic Constant: 7.09 V/in/sec
 - b) Resistance: 5652 Ohms
 - c) Calibration Constant: 40.1 KDynes/Ampere
 - d) Frequency (fo): 0.98 Hz
 - e) Open circuit damping (bo): 0.28 of critical damping
 - f) Suspended mass (m): 969.4 grams
 - g) Polarity: Negative voltage at socket E with respect to socket F when suspended mass moves toward to the case bottom

4. **Signal Coil (Longitudinal Detector)** Serial Number: 0508725
 - a) Electrodynamic Constant: 7.05 V/in/sec
 - b) Resistance: 5644 Ohms
 - c) Calibration Constant: 39.6 KDynes/Ampere
 - d) Frequency (fo): 0.96 Hz
 - e) Open circuit damping (bo): 0.285 of critical damping
 - f) Suspended mass (m): 969.9 grams
 - g) Polarity: Negative voltage at socket C with respect to socket D when suspended mass moves toward to the case bottom

5. **Signal Coil (Transverse Detector)** Serial Number: 0508726
 - a) Electrodynamic Constant: 7.24 V/in/sec
 - b) Resistance: 5647 Ohms
 - c) Calibration Constant: 40.5 KDynes/Ampere
 - d) Frequency (fo): 0.99 Hz
 - e) Open circuit damping (bo): 0.274 of critical damping
 - f) Suspended mass (m): 968.4 grams
 - g) Polarity: Negative voltage at socket G with respect to socket H when suspended mass moves toward to the case bottom

Figure 62. L4-3D L41161 factory calibration specifications.

1. **General**
 - a) Serial Number: L41162
 - b) Tested at 76 ° F
 - c) Leakage to case >100 Megohms at 500 volts.

2. **Calibration Coils, In Series**
 - a) Resistance: 20.9 Ohms
 - b) Polarity: Negative voltage at socket A with respect to socket B
when suspended mass moves toward to the case bottom

3. **Signal Coil (Vertical Detector)** Serial Number: L41172
 - a) Electrodynamc Constant: 7.1 V/in/sec
 - b) Resistance: 5649 Ohms
 - c) Calibration Constant: 40.4 KDynes/Ampere
 - d) Frequency (fo): 0.98 Hz
 - e) Open circuit damping (bo): 0.287 of critical damping
 - f) Suspended mass (m): 966.8 grams
 - g) Polarity: Negative voltage at socket E with respect to socket F
when suspended mass moves toward to the case bottom

4. **Signal Coil (Longitudinal Detector)** Serial Number: 508727
 - a) Electrodynamc Constant: 6.93 V/in/sec
 - b) Resistance: 5647 Ohms
 - c) Calibration Constant: 40.3 KDynes/Ampere
 - d) Frequency (fo): 0.98 Hz
 - e) Open circuit damping (bo): 0.288 of critical damping
 - f) Suspended mass (m): 971.3 grams
 - g) Polarity: Negative voltage at socket C with respect to socket D
when suspended mass moves toward to the case bottom

5. **Signal Coil (Transverse Detector)** Serial Number: 508728
 - a) Electrodynamc Constant: 7.27 V/in/sec
 - b) Resistance: 5645 Ohms
 - c) Calibration Constant: 39.2 KDynes/Ampere
 - d) Frequency (fo): 0.96 Hz
 - e) Open circuit damping (bo): 0.273 of critical damping
 - f) Suspended mass (m): 970.7 grams
 - g) Polarity: Negative voltage at socket G with respect to socket H
when suspended mass moves toward to the case bottom

Figure 63. L4-3D L41162 factory calibration specifications.

1. **General**
 - a) Serial Number: L41163
 - b) Tested at 78 ° F
 - c) Leakage to case >100 Megohms at 500 volts.

2. **Calibration Coils, In Series**
 - a) Resistance: 20.2 Ohms
 - b) Polarity: Negative voltage at socket A with respect to socket B
when suspended mass moves toward to the case bottom

3. **Signal Coil (Vertical Detector)** Serial Number: L41173
 - a) Electrodynamical Constant: 7.14 V/in/sec
 - b) Resistance: 5638 Ohms
 - c) Calibration Constant: 41.4 KDynes/Ampere
 - d) Frequency (fo): 1 Hz
 - e) Open circuit damping (bo): 0.276 of critical damping
 - f) Suspended mass (m): 967.2 grams
 - g) Polarity: Negative voltage at socket E with respect to socket F
when suspended mass moves toward to the case bottom

4. **Signal Coil (Longitudinal Detector)** Serial Number: 508729
 - a) Electrodynamical Constant: 7.29 V/in/sec
 - b) Resistance: 5636 Ohms
 - c) Calibration Constant: 41.2 KDynes/Ampere
 - d) Frequency (fo): 1.01 Hz
 - e) Open circuit damping (bo): 0.276 of critical damping
 - f) Suspended mass (m): 970.7 grams
 - g) Polarity: Negative voltage at socket C with respect to socket D
when suspended mass moves toward to the case bottom

5. **Signal Coil (Transverse Detector)** Serial Number: 508730
 - a) Electrodynamical Constant: 7.24 V/in/sec
 - b) Resistance: 5622 Ohms
 - c) Calibration Constant: 40.9 KDynes/Ampere
 - d) Frequency (fo): 1 Hz
 - e) Open circuit damping (bo): 0.275 of critical damping
 - f) Suspended mass (m): 966.7 grams
 - g) Polarity: Negative voltage at socket G with respect to socket H
when suspended mass moves toward to the case bottom

Figure 64. L4-3D L41163 factory calibration specifications.

1. **General**
 - a) Serial Number: L41164
 - b) Tested at 79° F
 - c) Leakage to case >100 Megohms at 500 volts.

2. **Calibration Coils, In Series**
 - a) Resistance: 19.9 Ohms
 - b) Polarity: Negative voltage at socket A with respect to socket B
when suspended mass moves toward to the case bottom

3. **Signal Coil (Vertical Detector)** Serial Number: L41174
 - a) Electrodynamical Constant: 7.26 V/in/sec
 - b) Resistance: 5630 Ohms
 - c) Calibration Constant: 41.5 KDynes/Ampere
 - d) Frequency (fo): 0.99 Hz
 - e) Open circuit damping (bo): 0.283 of critical damping
 - f) Suspended mass (m): 974.5 grams
 - g) Polarity: Negative voltage at socket E with respect to socket F
when suspended mass moves toward to the case bottom

4. **Signal Coil (Longitudinal Detector)** Serial Number: 508731
 - a) Electrodynamical Constant: 7.28 V/in/sec
 - b) Resistance: 5637 Ohms
 - c) Calibration Constant: 39.2 KDynes/Ampere
 - d) Frequency (fo): 0.96 Hz
 - e) Open circuit damping (bo): 0.268 of critical damping
 - f) Suspended mass (m): 971.6 grams
 - g) Polarity: Negative voltage at socket C with respect to socket D
when suspended mass moves toward to the case bottom

5. **Signal Coil (Transverse Detector)** Serial Number: 508732
 - a) Electrodynamical Constant: 7.25 V/in/sec
 - b) Resistance: 5636 Ohms
 - c) Calibration Constant: 39.3 KDynes/Ampere
 - d) Frequency (fo): 0.97 Hz
 - e) Open circuit damping (bo): 0.283 of critical damping
 - f) Suspended mass (m): 969 grams
 - g) Polarity: Negative voltage at socket G with respect to socket H
when suspended mass moves toward to the case bottom

Figure 65. L4-3D L41164 factory calibration specifications.

1. **General**
 - a) Serial Number: L41165
 - b) Tested at 78 ° F
 - c) Leakage to case >100 Megohms at 500 volts.

2. **Calibration Coils, In Series**
 - a) Resistance: 20.5 Ohms
 - b) Polarity: Negative voltage at socket A with respect to socket B
when suspended mass moves toward to the case bottom

3. **Signal Coil (Vertical Detector)** Serial Number: L41175
 - a) Electrodynamc Constant: 7.05 V/in/sec
 - b) Resistance: 5636 Ohms
 - c) Calibration Constant: 41.2 KDynes/Ampere
 - d) Frequency (fo): 0.98 Hz
 - e) Open circuit damping (bo): 0.277 of critical damping
 - f) Suspended mass (m): 970.2 grams
 - g) Polarity: Negative voltage at socket E with respect to socket F
when suspended mass moves toward to the case bottom

4. **Signal Coil (Longitudinal Detector)** Serial Number: 508733
 - a) Electrodynamc Constant: 7.21 V/in/sec
 - b) Resistance: 5633 Ohms
 - c) Calibration Constant: 39.6 KDynes/Ampere
 - d) Frequency (fo): 0.98 Hz
 - e) Open circuit damping (bo): 0.275 of critical damping
 - f) Suspended mass (m): 972.5 grams
 - g) Polarity: Negative voltage at socket C with respect to socket D
when suspended mass moves toward to the case bottom

5. **Signal Coil (Transverse Detector)** Serial Number: 508734
 - a) Electrodynamc Constant: 7.1 V/in/sec
 - b) Resistance: 5613 Ohms
 - c) Calibration Constant: 41.9 KDynes/Ampere
 - d) Frequency (fo): 1 Hz
 - e) Open circuit damping (bo): 0.274 of critical damping
 - f) Suspended mass (m): 972.1 grams
 - g) Polarity: Negative voltage at socket G with respect to socket H
when suspended mass moves toward to the case bottom

Figure 66. L4-3D L41165 factory calibration specifications.

1. **General**
 - a) Serial Number: L41166
 - b) Tested at 79 ° F
 - c) Leakage to case >100 Megohms at 500 volts.

2. **Calibration Coils, In Series**
 - a) Resistance: 22 Ohms
 - b) Polarity: Negative voltage at socket A with respect to socket B
when suspended mass moves toward to the case bottom

3. **Signal Coil (Vertical Detector)** Serial Number: L41176
 - a) Electrodynamc Constant: 7.15 V/in/sec
 - b) Resistance: 5637 Ohms
 - c) Calibration Constant: 40.2 KDynes/Ampere
 - d) Frequency (fo): 0.98 Hz
 - e) Open circuit damping (bo): 0.272 of critical damping
 - f) Suspended mass (m): 969.3 grams
 - g) Polarity: Negative voltage at socket E with respect to socket F
when suspended mass moves toward to the case bottom

4. **Signal Coil (Longitudinal Detector)** Serial Number: 508735
 - a) Electrodynamc Constant: 7.33 V/in/sec
 - b) Resistance: 5653 Ohms
 - c) Calibration Constant: 39.7 KDynes/Ampere
 - d) Frequency (fo): 1 Hz
 - e) Open circuit damping (bo): 0.284 of critical damping
 - f) Suspended mass (m): 971.9 grams
 - g) Polarity: Negative voltage at socket C with respect to socket D
when suspended mass moves toward to the case bottom

5. **Signal Coil (Transverse Detector)** Serial Number: 508736
 - a) Electrodynamc Constant: 7.3 V/in/sec
 - b) Resistance: 5646 Ohms
 - c) Calibration Constant: 40.3 KDynes/Ampere
 - d) Frequency (fo): 0.99 Hz
 - e) Open circuit damping (bo): 0.273 of critical damping
 - f) Suspended mass (m): 971.8 grams
 - g) Polarity: Negative voltage at socket G with respect to socket H
when suspended mass moves toward to the case bottom

Figure 67. L4-3D L41166 factory calibration specifications.

1. **General**
 - a) Serial Number: L41167
 - b) Tested at 81 ° F
 - c) Leakage to case >100 Megohms at 500 volts.

2. **Calibration Coils, in Series**
 - a) Resistance: 31.9 Ohms
 - b) Polarity: Negative voltage at socket A with respect to socket B when suspended mass moves toward to the case bottom

3. **Signal Coil (Vertical Detector)** Serial Number: L41177
 - a) Electrodynamc Constant: 7.12 V/in/sec
 - b) Resistance: 5674 Ohms
 - c) Calibration Constant: 40.9 KDynes/Ampere
 - d) Frequency (fo): 1 Hz
 - e) Open circuit damping (bo): 0.28 of critical damping
 - f) Suspended mass (m): 971.6 grams
 - g) Polarity: Negative voltage at socket E with respect to socket F when suspended mass moves toward to the case bottom

4. **Signal Coil (Longitudinal Detector)** Serial Number: 508737
 - a) Electrodynamc Constant: 7.36 V/in/sec
 - b) Resistance: 5694 Ohms
 - c) Calibration Constant: 39.6 KDynes/Ampere
 - d) Frequency (fo): 0.99 Hz
 - e) Open circuit damping (bo): 0.279 of critical damping
 - f) Suspended mass (m): 972.8 grams
 - g) Polarity: Negative voltage at socket C with respect to socket D when suspended mass moves toward to the case bottom

5. **Signal Coil (Transverse Detector)** Serial Number: 508738
 - a) Electrodynamc Constant: 7.13 V/in/sec
 - b) Resistance: 5676 Ohms
 - c) Calibration Constant: 41.6 KDynes/Ampere
 - d) Frequency (fo): 1 Hz
 - e) Open circuit damping (bo): 0.271 of critical damping
 - f) Suspended mass (m): 969.5 grams
 - g) Polarity: Negative voltage at socket G with respect to socket H when suspended mass moves toward to the case bottom

Figure 68. L4-3D L41167 factory calibration specifications.

1. **General**
 - a) Serial Number: L41168
 - b) Tested at 81 ° F
 - c) Leakage to case >100 Megohms at 500 volts.

2. **Calibration Coils, In Series**
 - a) Resistance: 22.4 Ohms
 - b) Polarity: Negative voltage at socket A with respect to socket B
when suspended mass moves toward to the case bottom

3. **Signal Coil (Vertical Detector)** Serial Number: L41178
 - a) Electrodynamc Constant: 7.05 V/in/sec
 - b) Resistance: 5646 Ohms
 - c) Calibration Constant: 41.1 KDynes/Ampere
 - d) Frequency (fo): 0.98 Hz
 - e) Open circuit damping (bo): 0.289 of critical damping
 - f) Suspended mass (m): 966.8 grams
 - g) Polarity: Negative voltage at socket E with respect to socket F
when suspended mass moves toward to the case bottom

4. **Signal Coil (Longitudinal Detector)** Serial Number: 508739
 - a) Electrodynamc Constant: 7.23 V/in/sec
 - b) Resistance: 5676 Ohms
 - c) Calibration Constant: 40.4 KDynes/Ampere
 - d) Frequency (fo): 1 Hz
 - e) Open circuit damping (bo): 0.266 of critical damping
 - f) Suspended mass (m): 974.4 grams
 - g) Polarity: Negative voltage at socket C with respect to socket D
when suspended mass moves toward to the case bottom

5. **Signal Coil (Transverse Detector)** Serial Number: 508740
 - a) Electrodynamc Constant: 7.25 V/in/sec
 - b) Resistance: 5669 Ohms
 - c) Calibration Constant: 41.8 KDynes/Ampere
 - d) Frequency (fo): 1 Hz
 - e) Open circuit damping (bo): 0.274 of critical damping
 - f) Suspended mass (m): 971.3 grams
 - g) Polarity: Negative voltage at socket G with respect to socket H
when suspended mass moves toward to the case bottom

Figure 69. L4-3D L41168 factory calibration specifications.

1. **General**
 - a) Serial Number: L41169
 - b) Tested at 75 ° F
 - c) Leakage to case >100 Megohms at 500 volts.

2. **Calibration Coils, In Series**
 - a) Resistance: 23.8 Ohms
 - b) Polarity: Negative voltage at socket A with respect to socket B
when suspended mass moves toward to the case bottom

3. **Signal Coil (Vertical Detector)** Serial Number: L41179
 - a) Electrodynamic Constant: 7.03 V/in/sec
 - b) Resistance: 5594 Ohms
 - c) Calibration Constant: 41 KDynes/Ampere
 - d) Frequency (fo): 0.97 Hz
 - e) Open circuit damping (bo): 0.28 of critical damping
 - f) Suspended mass (m): 970 grams
 - g) Polarity: Negative voltage at socket E with respect to socket F
when suspended mass moves toward to the case bottom

4. **Signal Coil (Longitudinal Detector)** Serial Number: Ø508741
 - a) Electrodynamic Constant: 6.93 V/in/sec
 - b) Resistance: 5672 Ohms
 - c) Calibration Constant: 44.5 KDynes/Ampere
 - d) Frequency (fo): 1 Hz
 - e) Open circuit damping (bo): 0.257 of critical damping
 - f) Suspended mass (m): 968.9 grams
 - g) Polarity: Negative voltage at socket C with respect to socket D
when suspended mass moves toward to the case bottom

5. **Signal Coil (Transverse Detector)** Serial Number: Ø508742
 - a) Electrodynamic Constant: 7.23 V/in/sec
 - b) Resistance: 5631 Ohms
 - c) Calibration Constant: 41.1 KDynes/Ampere
 - d) Frequency (fo): 1 Hz
 - e) Open circuit damping (bo): 0.271 of critical damping
 - f) Suspended mass (m): 972.7 grams
 - g) Polarity: Negative voltage at socket G with respect to socket H
when suspended mass moves toward to the case bottom

Figure 70. L4-3D L41169 factory calibration specifications.

1. **General**
 - a) Serial Number: L41170
 - b) Tested at 73 ° F
 - c) Leakage to case >100 Megohms at 500 volts.

2. **Calibration Coils, In Series**
 - a) Resistance: 23 Ohms
 - b) Polarity: Negative voltage at socket A with respect to socket B
when suspended mass moves toward to the case bottom

3. **Signal Coil (Vertical Detector)** Serial Number: L41180
 - a) Electrodynamical Constant: L41180 V/in/sec
 - b) Resistance: 5600 Ohms
 - c) Calibration Constant: 41.1 KDynes/Ampere
 - d) Frequency (fo): 0.96 Hz
 - e) Open circuit damping (bo): 0.283 of critical damping
 - f) Suspended mass (m): 964.8 grams
 - g) Polarity: Negative voltage at socket E with respect to socket F
when suspended mass moves toward to the case bottom

4. **Signal Coil (Longitudinal Detector)** Serial Number: 0508743
 - a) Electrodynamical Constant: 6.73 V/in/sec
 - b) Resistance: 5565 Ohms
 - c) Calibration Constant: 45.1 KDynes/Ampere
 - d) Frequency (fo): 1 Hz
 - e) Open circuit damping (bo): 0.257 of critical damping
 - f) Suspended mass (m): 972.8 grams
 - g) Polarity: Negative voltage at socket C with respect to socket D
when suspended mass moves toward to the case bottom

5. **Signal Coil (Transverse Detector)** Serial Number: 0508744
 - a) Electrodynamical Constant: 6.85 V/in/sec
 - b) Resistance: 5552 Ohms
 - c) Calibration Constant: 42.1 KDynes/Ampere
 - d) Frequency (fo): 0.98 Hz
 - e) Open circuit damping (bo): 0.283 of critical damping
 - f) Suspended mass (m): 972.2 grams
 - g) Polarity: Negative voltage at socket G with respect to socket H
when suspended mass moves toward to the case bottom

Figure 71. L4-3D L41170 factory calibration specifications.

APPENDIX D. DATA RECORDS WITH HIGH NOISE OR CONTAMINATION

Near-source

No near-source data had issues with noise or signal contamination when the data was examined in a band pass of 1 to 20 Hz.

Short Period

The following short period stations had signal quality problems due to the listed issue when the data was examined in a band pass of 1 to 20 Hz. Filtering can help with noise issues.

Table 14. Short Period Data Quality Issues.

Shot 1	Shot 2	Shot 3	Shot 4	Shot 5
NE10-Noise	NE08-Car prior to shot arrival	NE05-Noise, possibly from lawn mower	NE05-Noise, possibly from lawn mower	NE02-Car prior to shot arrival
SE03-Noise	NE09-Car	NE10-Noise	SE05-Car?	NE08-Car
SE07-Noise	SE05-Car			
SE10-Noise	SE09-Car			
	SE10-Noise			

Texan

The following Texan stations had signal quality problems due to the listed issue when the data was examined in a band pass of 4 to 20 Hz. Filtering can help with noise issues.

Table 15. Texan Data Quality Issues.

Shot 1	Shot 2	Shot 3	Shot 4	Shot 5
ST11-Cont	ST09-Cont	ST19-Cont	ST10-Cont	ST34-Bad
ST20-Noise	ST10-Cont	ST34-Bad	ST11-Cont	ST40-Cont
ST22-Cont	ST34-Bad	ST45-Noise	ST22-Cont	ST45-Noise
ST23-Cont	ST44-Cont	TN04-Bad	ST30-Cont	TN04-Bad
ST34-Bad	ST45-Noise	TN11-Noise	ST34-Bad	TN26-Cont
ST40-Noise	TN04-Bad	TN12-Cont	ST45-Noise	TN36-Noise
ST41-Noise	TN06-Cont	TN20-Noise	TN04-Bad	TN39-Cont
ST42-Noise	TN09-Noise	TN26-Cont	TN11-Cont	TN40-Noise
ST43-Noise	TN11-Cont	TN28-Cont	TN30-Cont	
ST44-Noise	TN30-Noise	TN39-Cont	TN38-Cont	
ST45-Noise	TN33-Noise	TN40-Noise	TN39-Noise	
TN04-Bad	TN34-Cont		TN40-Noise	
TN11-Noise				
TN25-Cont				
TN28-Cont				
TN30-Noise				
TN32-Cont				
TN33-Noise				
TN40-Cont				

Noise=High noise levels; Cont=Contamination by other unspecified signals; Bad=Geophone or cable connection was bad

APPENDIX E. BLASTER'S LOG FOR 11 JULY 2008 PRODUCTION SHOT



UNIFORM BLASTER'S LOG

Location of Blast <u>Rock of Ages</u>		GPS Information	
Street Address:		At shot	
City: <u>Berre VT</u>		At protected structure	
Date of Blast: <u>7-11-08</u>	Time of Blast: <u>3:40</u> <input type="checkbox"/> AM <input checked="" type="checkbox"/> PM	Description of Blast: <input type="checkbox"/> Construction <input type="checkbox"/> Quarry <input type="checkbox"/> Trench	

Weather Conditions

Conditions:
 Cloudy Clear Rain Snow
 Temperature: /Degree F 80 Wind Velocity: /MPH and Direction:

Design Information

Face Height: /ft	Over Burden: /ft <u>0'-2'</u>	Burden: /ft <u>5'</u>	Cubic yards <u>855</u>
Type of Material Blasted: <u>Granite</u>	Hole Diameter: /in <u>3 1/2"</u>	Spacing: /ft <u>5'</u>	Tons: <u>1890</u>
Hole Depth: /ft <u>7'-15'</u>	Deck Stem: /ft	Number of holes: <u>84 (7 rows)</u>	lbs/yr ³ <u>1.5</u>
Sub Drill: /ft	Type of Stemming: <u>crushed stone</u>	Collar Stem: /ft <u>5'-7'</u>	Tons /lb. <u>104</u>
Blast Mat / Cover Used: <u>none</u>	Drill Co. <u>Yankee</u>	Face Direction:	Total Drill footage: <u>1001</u>

Explosives Used

Type	1. <u>2 Procut</u>	2. <u>Presplit 7/8</u>	3. <u>Emgel 250 2x16</u>	4. <u>Emgel 250 2 3/4 x 16</u>
Lbs.	<u>84</u>	<u>55</u>	<u>220</u>	<u>990</u>
Type	5.	6.	7.	8.
Lbs.				
Max. holes per 8ms delay:		Max. lbs. per 8ms delay:		Total lbs: <u>1349</u>

Initiation System

Type of Initiation System
 Electric Non Electric Other: Sequential Machine CO Other:

ELECTRIC See attachments

Timer Setting Hole to Hole:	Nominal Cap Delay Hole to Hole:	Timer Setting Row to Row:	Cap Nominal Delay Row to Row:
Cap Delays per Circuit:	Number of Circuits:	OHMS: (Resistance each series or circuit)	

NON ELECTRIC (8 MS RULE) See attachments

Number of Rows: <u>7</u>	Delay(s) parallel to free face along spacing: <u>12</u>
Delay(s) Perpendicular to the face, in echelon or row to row: <u>7</u>	

Nearest Protected Structure

Street Address:

Type of Structure:	Distance: /ft
--------------------	---------------

Allowable Limits of Vibration

OPTION 1 OPTION 2

Scaled Distance:
 50 55 60 65 Other:

Post-It® Fax Note	7671	Date <u>7/29</u>	# of pages <u>1</u>
To <u>Jessie Bonner</u>	From <u>Don Murray</u>		
Co./Dept.	Co.		
Phone #	Phone #		
Fax # <u>936 632 4226</u>	Fax #		

(Conforms to M.G.L. c 14